3. System Operation

This section describes normal operation of the network instruments, methods to acquire and process data, and methodologies to characterize the SUV-100 spectroradiometers.

3.1. Types and Schedule of Spectral Measurements

There are five different types of instrument scans—Data, Response, Wavelength, Background, and Absolute scans. These types of scans are summarized in Table 3.1 and described in detail in the following sections.

Data scans measure solar irradiance while the rest are used for calibrations and quality control. *Response* scans determine system responsivity using the internal 45-Watt Tungsten-Halogen lamp as a source. They consist of one to six segments with the same PMT high voltage settings as those employed for that day's data scans - with the shutter closed and the internal 45-Watt response lamp energized. *Internal wavelength* scans and *external wavelength* scans are used to determine spectral bandwidth of the monochromator and wavelength registration utilizing Mercury discharge lamps. *Background* data are continuously logged to monitor the auxiliary sensors. *Absolute* scans are manually executed approximately biweekly (conditions permitting), and are performed to calibrate the system using an external 200-Watt Tungsten-Halogen standards of spectral irradiance. Finally, *user defined scans* are *also* performed during special events like intercomparison campaigns or site visits.

Table 3.1 Scan parameters used in the NSF Monitoring Network, 1998 revisions.

Scan	Wavelength increment	Range	Approx. Duration	Approximate File Size	Interval
Data Item 1	0.2 nm	280 to 345 nm	00:04:28		
Data Item 2	0.5 nm	335 to 405 nm	00:01:56		
Data Item 3	1.0 nm	395 to 605 nm	00:03:04		
Data Item 4	0.5 nm	280 to 290 nm	00:00:17		
Total Data			13 min	8 Kbytes	15 min
Response	1.0 nm	280-605	00:05:06 per item (1 to 6 per day) plus 5 min. lamp warm-up	Up to 20 Kbytes	1 per day
Wavelength	0.1 nm	Segmented	16 min.	15 Kbytes	1 per day
Background	1 observation recorded/5 min.	N/A	< 00:00:01	73 Kbytes per day	Continuous, when other scans are not running.
Absolute	1.0 nm	250 to 700 nm	1 hour plus set-up time	71 Kbytes	Biweekly

Historically, the number of scans per day and the number of wavelengths measured per spectrum was a compromise between scientific needs, and the challenges of transmitting large blocks of data from remote locations. Communication facilities have improved over the years, and the scan schedule was adjusted accordingly. During the first months of the Volume 7 season (1997-1998), data were collected at a rate of two scans per hour, as in previous seasons. In the middle of the season a scan rate of four scans per hour during daylight was implemented at all sites. Typically only one scan per night is taken. At sites inside the polar circles (Barrow, McMurdo, and South Pole), the instrument operates on a reduced scan schedule during the extended periods of darkness in winter, typically one scan of each type (data, wavelength, and response) per day. For the purpose of accurate timekeeping, a GPS integral to the system is automatically referenced at least once daily, and the computer clock is updated accordingly.

A data scan is divided in separate scan segments, called "items", to allow measurements with different instrument sensitivity (i.e., different settings of the PMT high-voltage) in different spectral regions. At short wavelengths (280-345 nm) the highest sensitivity (or highest PMT voltage) is applied. If this sensitivity were maintained beyond 345 nm, the instrument would saturate. Therefore, a smaller sensitivity is applied for the Item 2 and 3 segments. The Item 4 segment is a *dark* scan, see Section 3.2.1.

Since the start of network operation in 1988, several changes have been made in the scanning parameters. The data scan item 2 segment upper limit was increased first from 350 nm to 380 nm (1994-95), and again to 405 nm (1996) to further increase resolution into the UV-A to visible band. These extensions required reductions in sensitivity to avoid saturation. The slight loss of sensitivity when the segment was extended up to 405 nm in 1996 was more than compensated for by introduction of a new feature into the SUV-100 System Control Software that allows diurnal changes in PMT high voltage as a function of solar zenith angle. This resulted in maintenance of an optimum sensitivity throughout the day. The terminal wavelength for the item 3 scan was also reduced from 700 to 620 nm (1994-95) and again to 605 nm (1996). The system sensitivity at wavelengths longer than 600 nm is poor due to the monochromator and PMT optimization for the ultraviolet. In examining the data, we found that this sensitivity was so poor that we advise users to ignore data beyond 600 nm. A change to the wavelength increment of the item 3 segment was in response to requests of data users. In the 1991-1992 season, the increment was changed from 5 nm to 2.5 nm, and during the 1992-1993 season, it was further reduced to 1 nm.

During the 1994-1995 season site visits, all sites were upgraded with additional auxiliary channels (e.g., various temperature, humidity, and ground sensors) to better monitor system performance. Combined with computer and software upgrades in 1996-1997, this resulted in increases in daily data transmissions from each site. The total size of daily archives ranged up to 400 Kbytes in Volume 6. The change of the scan rate from 2 scans to 4 scans per hour during the Volume 7 season approximately doubled this number. Now the transfer from high latitude sites is approximately 350 Kbytes per day when measurements are performed 24 hours per day. During Polar Night the file size drops to about 20 Kbytes per day. The amount of data collected in San Diego is about 250 Kbytes per day throughout the year.

3.2. Scan Descriptions with Examples

Data scans are performed every 15 minutes indexed at the top of the hour, when the Sun is above the horizon. Under standard conditions, the wavelength and response scans are performed once a day. The frequency of absolute calibration scan performance is typically biweekly, but depends on weather conditions, location, time of year, and system performance. In the 1997/98 season, the instruments ran generally very stable and therefore the biweekly schedule could be applied with almost no exceptions. Other than these three major types of scans, some specially defined absolute scans, external mercury lamp scans, dark scans, for example, may be performed in frequencies ranging from several times daily to once a season.

The following sections describe the current mode of operation. In the 1997/98 season a schedule similar to the 1995-97 period was applied, except for the increased rate of data scans. For a detailed description of the earlier modes of operation, see the previous network operation reports.

3.2.1. Data Scan

A data scan measures solar radiation. A typical data scan is shown in Figure 3.1. As mentioned above, it is necessary to split a data scan in several segments to account for different instrument sensitivity requirement in different spectral regions. Between 280 and 345 nm, solar data is sampled in 0.2 nm steps (Item 1); between 335 and 405 nm the increment is 0.5 nm (Item 2). Item 3 is sampled in 1.0 nm steps between 395 to 605 nm (which includes most of the Photosynthetically Active Radiation (PAR) or "visible" spectrum).

In the course of data evaluation, the PMT dark current (i.e., the PMT current without radiation falling on the PMT's photo-cathode) has to be subtracted from the measurements (see Section 3.3.3.). Since there is no detectable solar radiation impinging the Earth's surface with wavelength below 290 nm, the dark current assigned to Item 1 is simply the average of measurements between 280-290 nm calculated from the same segment. However, this value cannot be used for Items 2 and 3 because of the different high voltages applied in these segments. A data scan consequently also includes a fourth item; a scan between 280 and 290 nm in 0.5 nm steps carried out with the same PMT high-voltage setting as for the Items 2 and 3. Since the PMT dark currents are measured with the shutter open, stray light (e.g., photons with wavelengths

above 290 nm that are registered at a smaller wavelengths) may also fall on the PMT cathode. Systematic errors in the measurement due to stray light (if they existed), are therefore partly reduced when subtracting the dark current from the Item 1-3 segments.

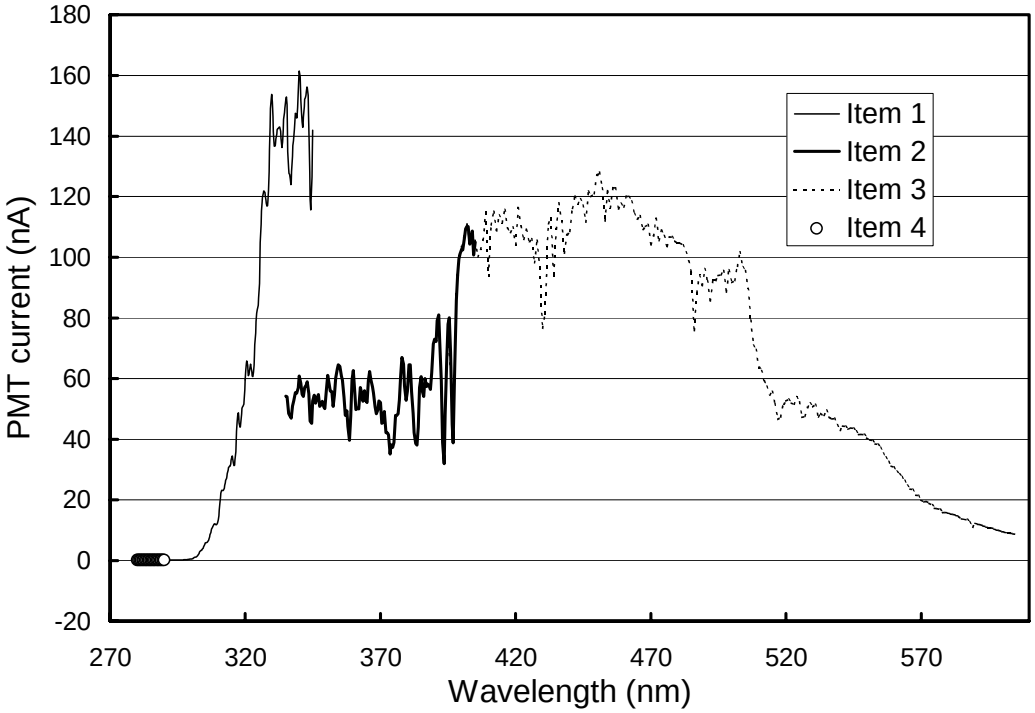

Figure 3.1. *PMT current before conversion to irradiance. Item 1 covers the spectral range 280-345 nm, Item 2 includes the range 335-405 nm, and Item 3 is from 395 to 605 nm. Item 1 is measured with a higher PMT voltage than Items 2 and 3. Item 4 (280-290 nm) is a measurement of the PMT dark current with the same voltage applied as for Items 2 and 3.*

At the beginning of Item 2, a delay of about 1-minute is specified to allow the PMT to stabilize at the new high voltage setting. The shutter is opened to allow solar irradiance to reach the monochromator and the sequence is started. A typical data scan takes about 13 minutes to complete. PMT high voltage setting is diurnally optimized to produce a maximum dynamic range without overload. These automatic adjustments can result in the use of one to six different PMT high-voltage sets per day, dependent on time-of-year and location. Spectral irradiance values, calculated from the data scan, are displayed in Figure 3.2 (linear y-axis) and Figure 3.3 (logarithmic y-axis).

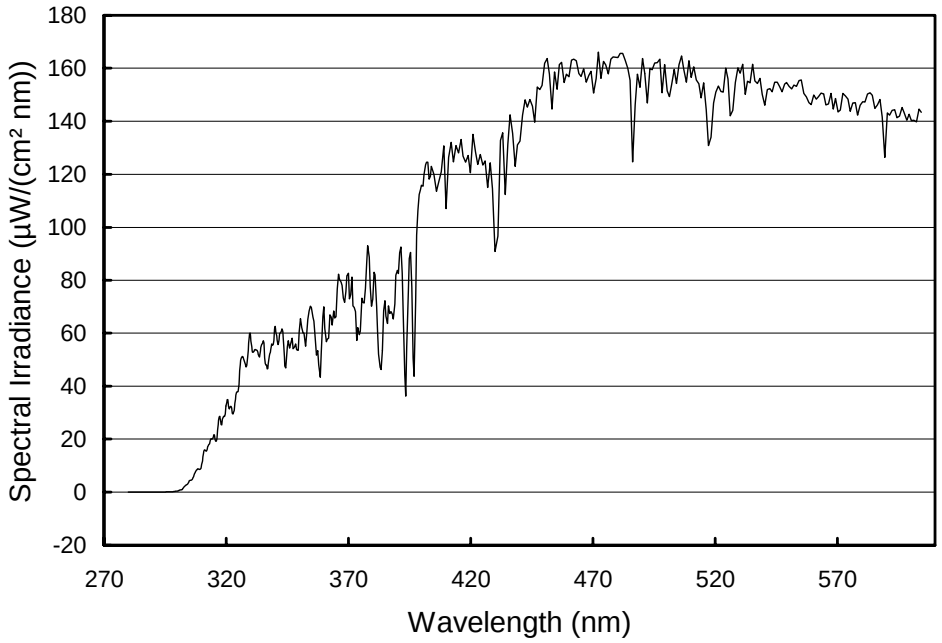

Figure 3.2. *Irradiance calculated from the PMT currents shown in the previous figure. Data from all three scan items are included.*

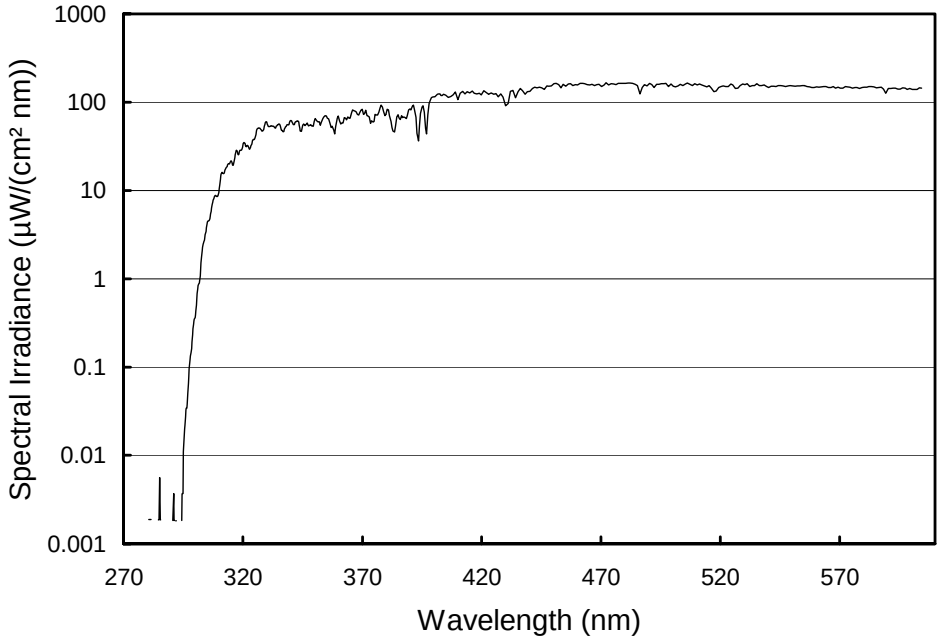

Figure 3.3. *Spectral irradiance from the previous figure but presented on logarithmic y-axis to demonstrate the steep decline of the solar spectrum in the UV-B.*

3.2.2. Response Scan

A response scan, normally scheduled for occurrence once a day, is used to track system responsivity by scanning a 45-Watt tungsten-halogen response lamp, internal to the SUV-100. To optimize system responsivity throughout the day, the data scan PMT high voltages are automatically adjusted as a function of solar zenith angle. The corresponding response scan consists of one to six items using the same system and PMT high-voltage settings (in 50 volt increments), as used during that day's data scans, with the shutter closed and response lamp energized. Prior to initiating the scan segment(s), a 5-minute lamp stabilization period following power-up ensures that the lamp reaches thermal equilibrium before the scan. After the "warm-up" period, the lamp drive current is then adjusted to a target setting. Figure 3.4 shows typical data recorded from a response scan. The lines represent PMT currents as a function of wavelength for a six-item response scan, at the various sensitivities (PMT high voltages) used in a single diurnal cycle. For quality control purpose, TSI sensor readings and the response lamp drive current are also recorded during a response scan. These parameters are reviewed to ensure that there are no response lamp changes during these scans.

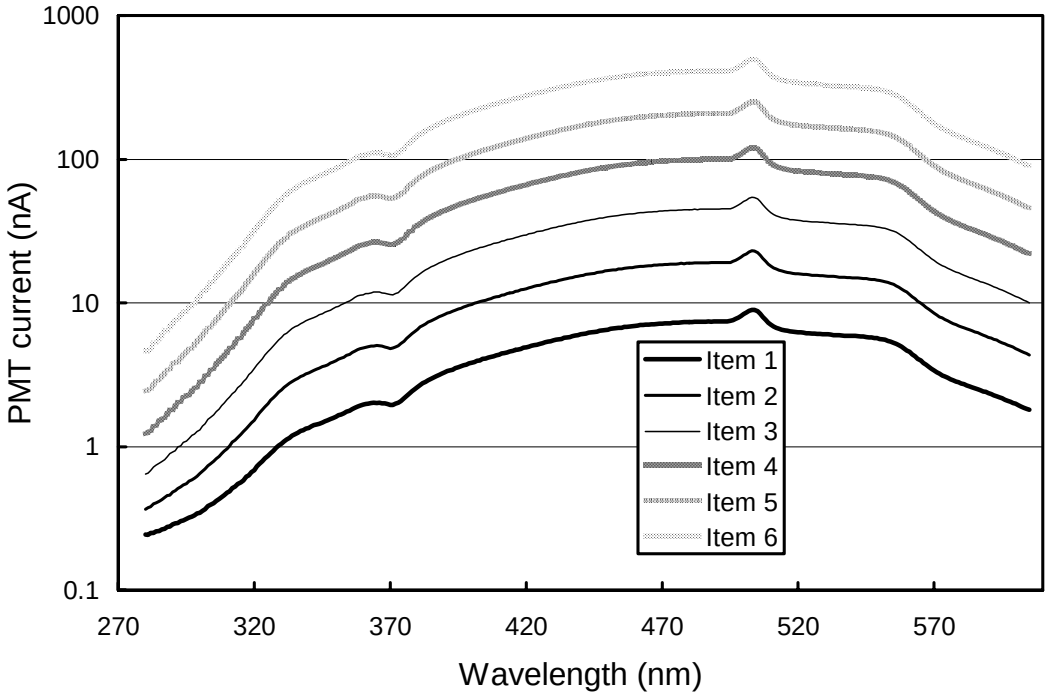

Figure 3.4. *Typical Response scan. Maximum PMT current may reach 1000 nA when the system is operated at peak sensitivity. The PMT dark current was not subtracted.*

3.2.3. Internal Wavelength Scan

Wavelength scans with the built-in mercury lamp are carried out in order to align the wavelength position reported by the system to the actual wavelength of photons passing the monochromator. In addition, wavelength scans allow the user to determine the bandpass (or bandwidth) of the monochromator. A wavelength scan is scheduled for once per day execution. The wavelength scan is composed of a series of segments, with the shutter closed and the internal Mercury discharge lamp energized. The segments are chosen to concentrate high spectral resolution scanning in areas throughout the spectroradiometer's sensitive range, where significant Mercury lamp lines occur. The PMT high voltage settings for each segment are optimized to maximize signal-to-noise ratio and linearity without overload (e.g., the PMT current is limited to approximately 500 - 700 nA at the 253.65 nm peak). The band shape of a typical

253.65 nm segment should resemble that shown in Figure 3.5. A malfunctioning of the monochromator would distort the shape of the line, causing side lobes resembling smaller peaks. A normal multiple-item scan is shown in Figure 3.6.

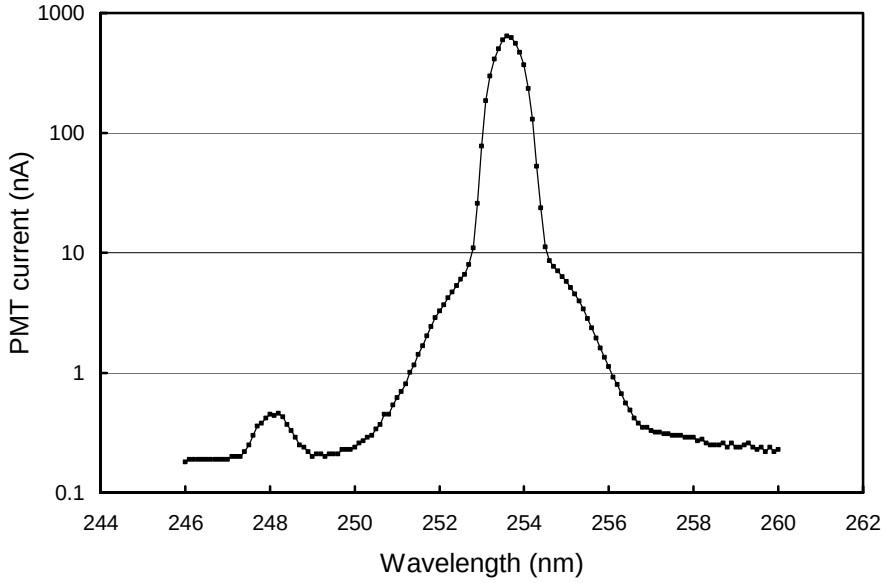

Figure 3.5. *Wavelength scan in the vicinity of the Mercury peak at 253.65 nm. Blocks indicate the individual measurements. No dark value has been subtracted, and the data has not been corrected for the monochromator offset. The small peak at 248 nm is from a weaker Mercury line.*

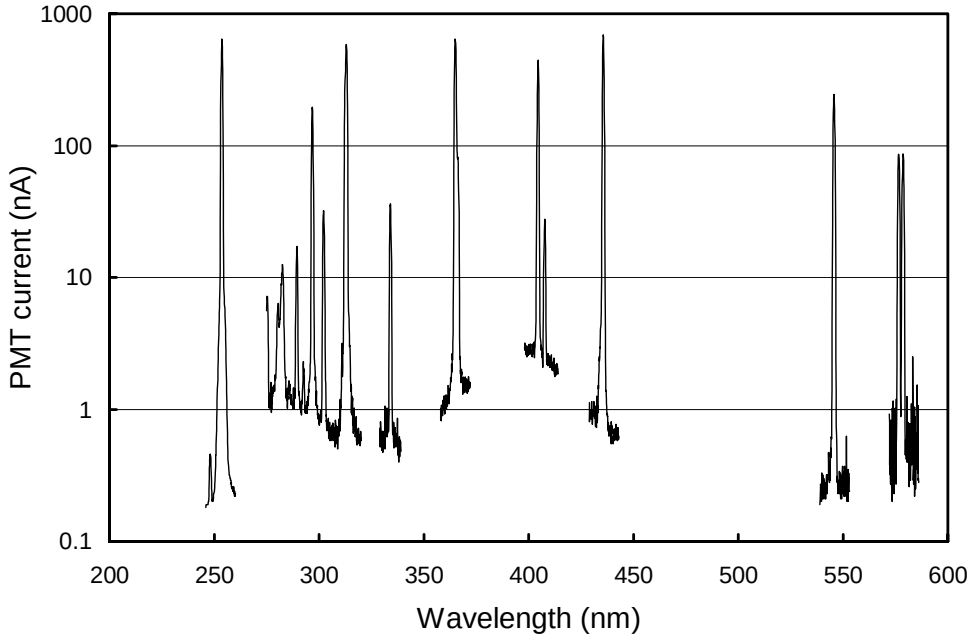

Figure 3.6. *Typical multi-peak Wavelength scan showing eight segments. The vertical axis indicates PMT current from the Mercury lamp on a logarithmic scale. The dark PMT current has not been subtracted. In a typical wavelength scan, the baseline value may show variation across the spectrum due to fluorescence from the lamp.*

3.2.4. Absolute Scan

The chief purpose of the absolute scans is to characterize the internal response lamp by comparison with a 200-Watt Tungsten-Halogen standard of spectral irradiance. For information on apparatus employed and application description, see Section 2.2.2. Under normal circumstances (i.e., when the system is stable and operating properly) these scans are performed biweekly. Each scan consists of eight segments, where the first four items characterize system behavior at short wavelengths (250-330 nm), and the last four segments characterize behavior between 250 nm and 700 nm. The reason for having two sets of four items is to optimize the system sensitivity via PMT high voltages for different parts of the spectrum. Each of the two sets has the following segments:

- Item 1 (or 5) is performed with the lamps turned off and the shutter open; it measures PMT dark current for the following 200-Watt lamp scan and detects any light leaks.
- Item 2 (or 6) is performed with the 200-Watt lamp on and the shutter open.
- Item 3 (or 7) is performed with the 45-Watt lamp on and the shutter closed.
- Item 4 (or 8) is performed with the lamps turned off and the shutter closed; it characterizes PMT dark current.

Items 1 through 4 are run at the same PMT high voltage setting, and 5 through 8 are run at a lower high voltage setting. For calibration of the internal 45-Watt lamp, Items 1-4 are used in the 250-330 nm range; Items 5-8 cover the entire wavelength range.

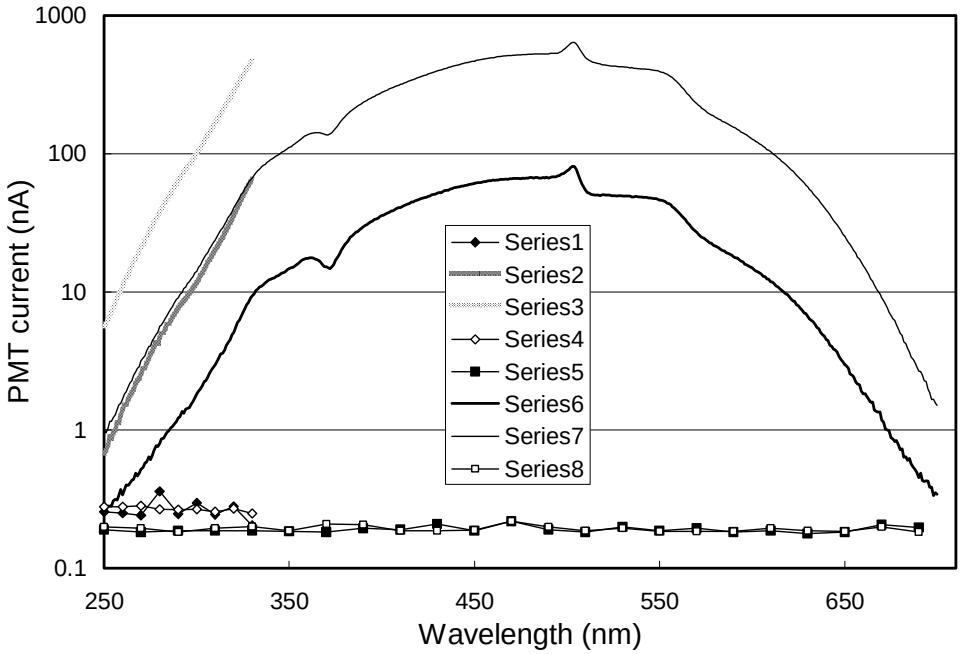

Figure 3.7. *Typical eight-item absolute scan. Note that the vertical axis has a logarithmic scale.*

3.2.5. External Wavelength Scan

It was discovered at the Boulder, Colorado 1994 intercomparison (Thompson et. al., 1997) that wavelength scans performed with internal and external sources differ due to different light paths for both scan types. Radiation from the internal Mercury lamp passes through two beam-splitters and enters the monochromator's entrance slit without further scattering. Radiation from an external Mercury source, however, is scattered first by the cosine collector before it enters the monochromator. Due to the different geometries the monochromators gratings are illuminated differently causing the deviation observed in the

wavelength registration. Beginning with the site visits of the 1994-1995 season, external wavelength scans have therefore been performed as a routine part of the site visit. These scans allow a more realistic measurement of the systems' bandpass and wavelength mapping because the light path of external scans is the same as for measurements of solar irradiance.

During the external wavelength scan, a Mercury lamp (or alternatively a Cadmium lamp or HeCd laser) is situated so that it fills the entire field-of-view of the collector. The external wavelength scan is composed of a series of segments that mirror internal wavelength scan segments. The shutter is open and PMT high voltages are set optimally for the best signal-to-noise ratio. A comparison of typical external and internal Mercury scans is shown in Figure 3.8. As can be seen, the external scan has a larger bandpass and a slightly different shape than the internal one. Since the line center of a Mercury line is determined by calculating the average of the two wavelengths where the function approaches the half of its maximum (see Section 3.1.1 for details), wavelength mappings based on internal and external wavelengths will have an offset (approximately 0.1 nm at 300 nm). Historically, no attempt was made in the data processing to correct for these effects, i.e., the wavelength mapping was solely based on internal scans and the external scans were only used for documentation. For Volume 7 data, the bias was diminished by means of a correlation technique described in Section 3.3.1.2.

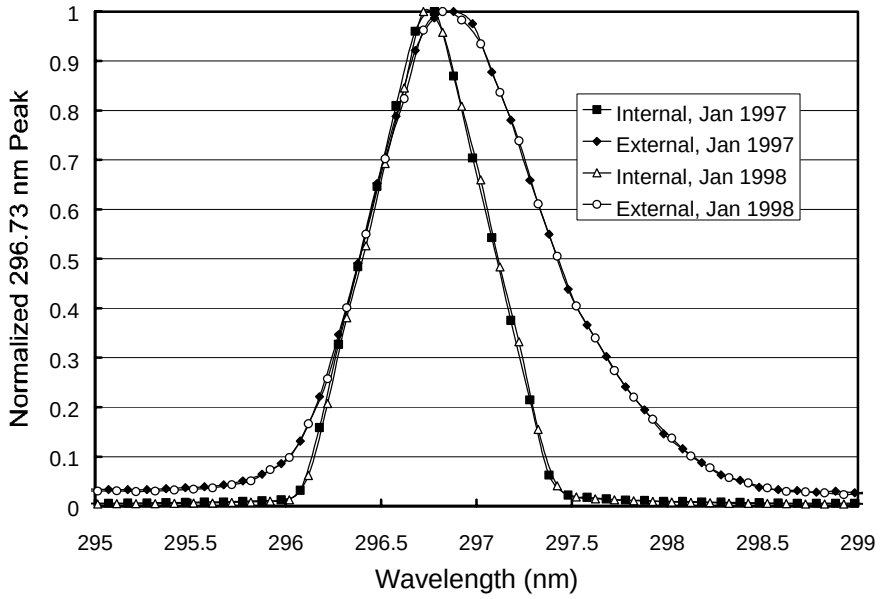

Figure 3.8. *Normalized Mercury peaks from external and internal wavelength scans. Data is from the 1997/98 McMurdo season.*

3.3. Calibration and Data Processing Protocols

This section describes the method used to calculate global spectral irradiance in units of μW/(cm^2 nm) from raw wavelength and PMT current data generated by the spectroradiometers. The wavelength calibration of the instruments is described in Section 3.3.1 and the irradiance calibration of data scans is explained in Section 3.3.2.

3.3.1. Wavelength Calibration and Correction

The wavelength calibration of Volume 1-6 network data was solely based on internal Mercury scans. The methodology applied is described in Section 3.3.1.1. For Volume 7, the algorithm has been changed, see

Section 3.3.1.2. The "old" method is presented here to document how a time-series spanning several volumes of data may be affected by the implementation of a new procedure.

3.3.1.1. Wavelength Calibration and Correction with Internal Mercury Scans Implemented for Volume 1-6 Data

The internal low-pressure Mercury lamp produces a number of emission lines that are seen as high-intensity, very narrow spikes in the wavelength scan. The wavelengths of these lines are precisely fixed fundamentally, thus forming the basis of the calibration. The lines are located by scanning in small wavelength steps (0.1 nm) and looking for changes in the PMT signal that are significantly larger than the background noise (see Section 3.2.3.).

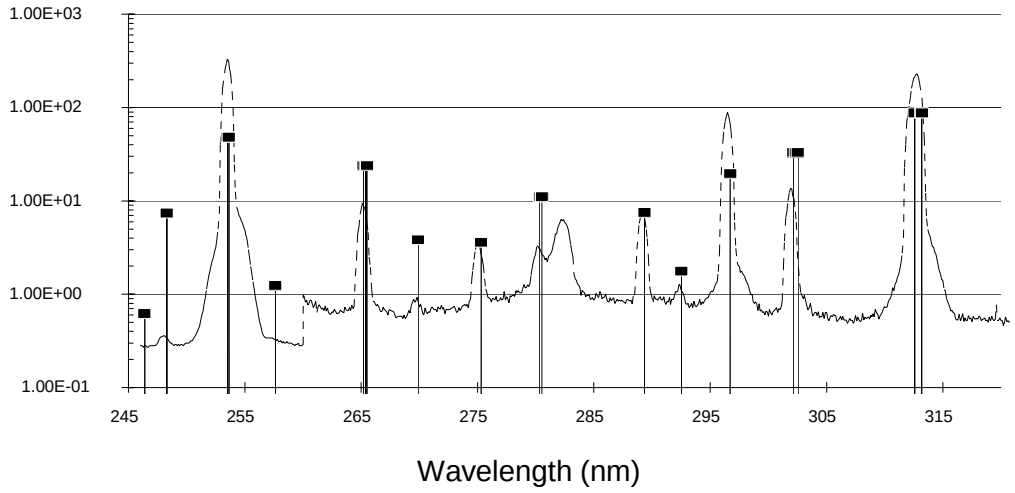

Figure 3.9. *Example of a Mercury lamp scan with an SUV-100 spectroradiometer (dashed line). Vertical lines represent the positions of the Mercury lines. Lines close together are caused by doublet or triplet emission lines.*

There are different methods of determining the exact location of a detected peak. These include the Full Width at Half-Maximum intensity "FWHM", "Tangent", and "Centroid" methods. All three methods produce almost identical results for single well-defined peaks. The biggest differences in results are expected in the cases of asymmetrical peaks.

The FWHM method starts with defining a threshold, usually twice the minimum PMT current (typically around 0.1 - 0.5 nA), and locating the maximum reading. Local maximums that are below the threshold are ignored. For each local maximum greater than the threshold, the location of the peak is computed. First, the two points closest in value to half of the maximum reading are identified on each side of the peak (see Wavelength (nm)
Figure 3.10). Interpolation between the two points on the left side leads to a half maximum wavelength position of λ_{left}, and interpolation between the two points on the right indicates a half maximum at λ_{right}. Finally, the distance between these half-maximum wavelengths defines the peak width, and the actual position of the peak is assumed to be $\frac{\lambda_{left} + \lambda_{right}}{2}$.

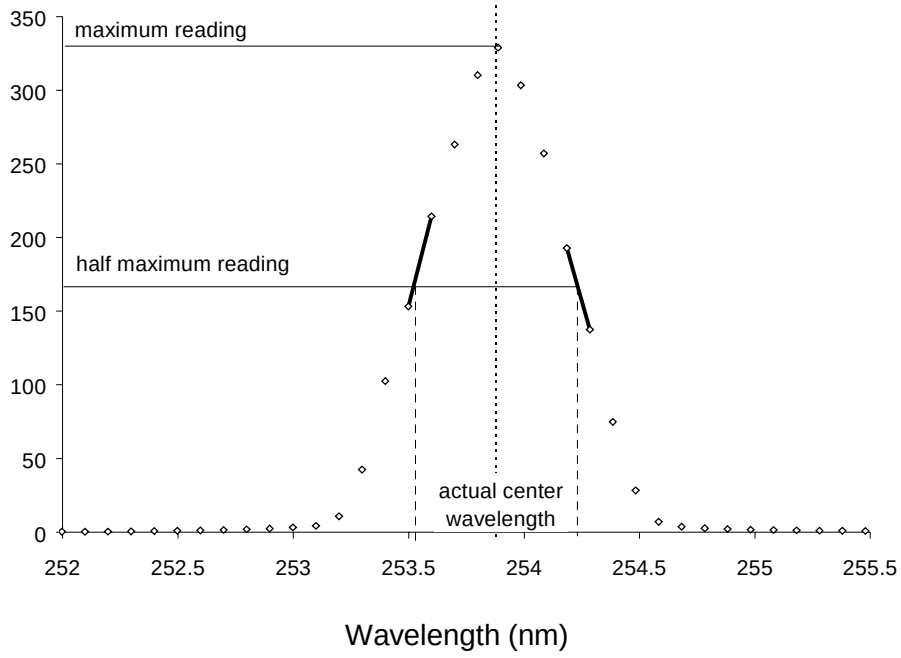

Figure 3.10. *Details of a single Hg peak along with the illustration of determining the center wavelength using the FWHM method.*

The FWHM method was historically used in our network data processing, but was replaced by the Tangent method in 1994. FWHM is useful and requires little effort (can be used manually) to obtain a satisfactory result. However, FWHM is known to produce unreasonable values on occasion, such as when there are multiple peaks close together or when the peak has small amplitude. Generally, the FWHM method does not accurately distinguish multiple peaks, and it yields significantly different estimates from the Tangent method on asymmetric peaks. A last disadvantage in using FWHM to process external wavelength scans is that it has a tendency to emphasize a peak's right shoulder (see Figure 3.8) when asymmetry exists.

The **Tangent method** involves extracting several reliable points on each side of the peak and drawing lines through them. More specifically, after finding a local maximum, seven points on each side of it are used in two linear regressions. The intersection of these two regression lines defines the peak location (see Figure 3.11). The primary reason for using seven points is that the bandwidth of the monochromator is known to be around 1.0 nm, and the number of 0.1 nm readings between two half maximums of most peaks is seven. Assuming the peak has a triangular shape, each side of the triangle is comprised of at least seven points. (Numerous wavelength scans verify existence of an optimal number of points between the maximum and inflection point). The advantage of this method is its computational simplicity based on convenience of recurrent procedures. Each local maximum location $\lambda_* \in (\lambda_1, \lambda_2)$ divides an interval into two smaller ones (λ_1, λ_*) and (λ_*, λ_2), where the search for local maximums is continued. The sequence ends when no maximum can be found. The tangent method is "insured" against producing an outlier, but it rejects some cases where peaks can be defined.

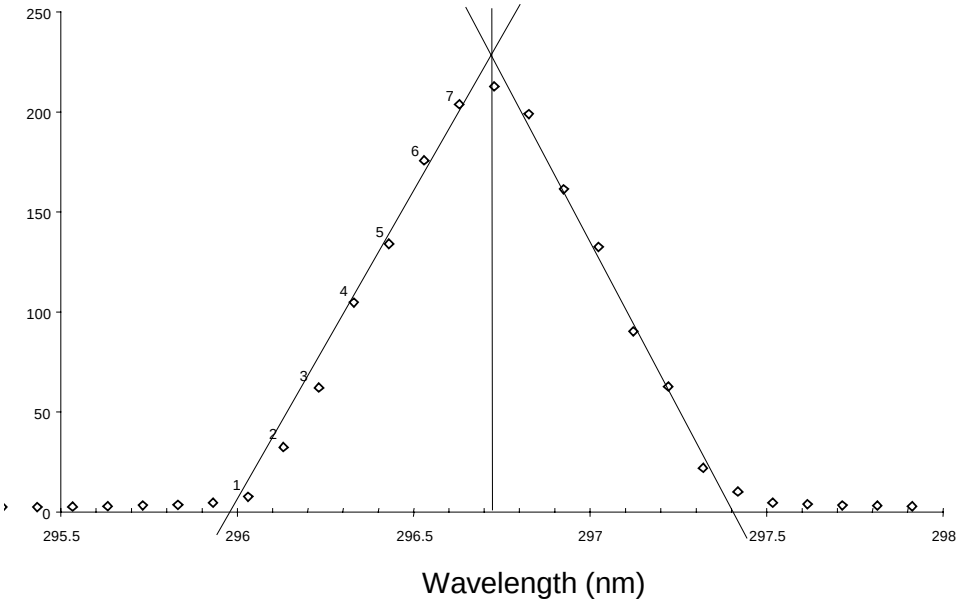

Figure 3.11. *Implementation of the Tangent method. Diamonds express PMT current of the mercury lamp in the 296-nm peak region. Intersection of the regressions (solid lines) defines center wavelength (dashed line).*

The **Centroid method** is used by NIST in some applications, and has been employed at intercomparisons. It is resultantly close to the FWHM method. This method is attractive due to its simple mathematical interpretation, but it is usually sensitive to the determination of the threshold, producing errors similar to those of the FWHM method. After a local maximum is detected at wavelength λ_* and a reasonable interval $\lambda_* \in (\lambda_0, \lambda_n)$ has been established, the actual peak location is defined as: $\lambda_* = \dfrac{\sum_{i=0}^{n} I(\lambda_i)\lambda_i}{\sum_{i=0}^{n} I(\lambda_i)}$, where $I(\lambda)$ is Hg lamp PMT current at that specific wavelength. The trick is to find the proper λ_0, λ_n. One of the procedures estimates boundaries as: $\lambda_0 = \min_{\substack{i \\ \lambda_i<\lambda_* \\ I(\lambda_i)>0.1I_{\max}}} \lambda_i$, $\lambda_n = \max_{\substack{i \\ \lambda_i>\lambda_* \\ I(\lambda_i)>0.1I_{\max}}} \lambda_i$, where I_{max} is the local maximum. The arbitrarily chosen multiple of 0.1 could just as well be substituted by any other value. Reducing this value obviously yields increased precision, but it also increases the risk of entering the domain of another peak, which is a real problem, as it drives λ_* out of the relevant interval. Wavelength (nm)

Figure 3.12 illustrates the difference in results obtained using the Centroid and Tangent methods.

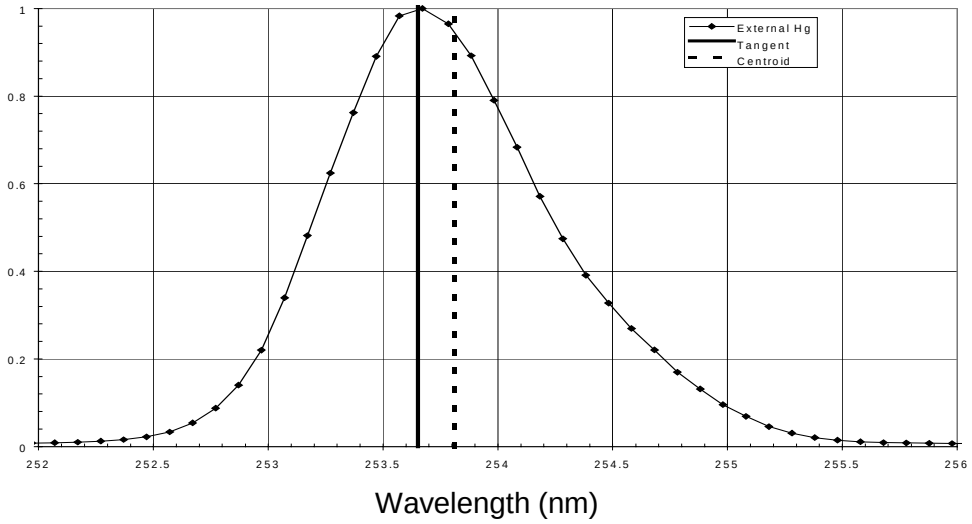

Figure 3.12. *Differences of the Tangent and Centroid methods. Diamonds express PMT current from the external wavelength scan in the 253 nm peak region; the heavy solid line represents the center wavelength as defined by the tangents method; and the dotted line is the result of the Centroid method. The difference between the two methods (about 0.15 nm) is caused by the well-pronounced right shoulder of the peak.*

The wavelength correction of data scans recorded in Volumes 1-6 was solely based on internal wavelength scans and can be described as a two-step process. In Step 1, the wavelength shift at the Mercury line of 296.728 nm is determined from the daily automatic wavelength scans with the internal Mercury lamp. The position of this line is determined by one of the methods described above. By subtracting the so determined wavelength from the desired wavelength, 296.728 nm, the wavelength shift is determined. This shift is then applied to the data scans (i.e., a whole spectrum is shifted by a constant value). After this step, the spectrum would be aligned correctly at 296.728 nm if the calibration with internal Mercury scans were without errors. Due to non-linearities in the monochromator's wavelength drive, however, Step 1 will not provide a correct wavelength alignment for the whole spectrum.

In Step 2 of the procedure, therefore, a shift-function is applied that is calculated from all Mercury lines of the wavelength scan. This function corrects for monochromator non-linearities. An example of this function is shown in Figure 3.13. The function is zero at 296.728 nm because it only describes wavelength deviations between measured and nominal wavelength positions relative to this wavelength. The function is usually very stable throughout a season and it is therefore calculated from the average of all wavelength scans performed during that season. The function is described by a series of linear equations of the form $\Delta\lambda = a_n + b_n\lambda$ (the constants a_n and b_n are offset and scale-factor) that are applied stepwise in different wavelength segments.

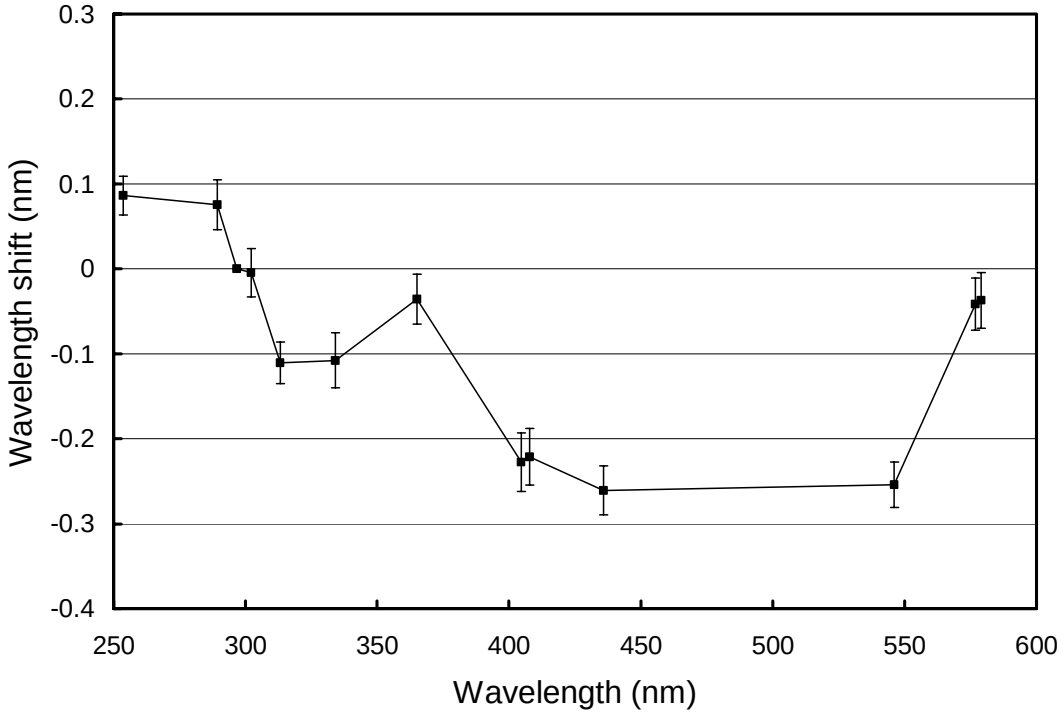

Figure 3.13. *Typical function expressing monochromator non-linearity. The plot is based on Palmer data from the Volume 7 season. Approximately 347 internal wavelength scans were evaluated. The error bars represent* $\pm 1\sigma$ *limits.*

In summary, Step 1 takes account of the day-to-day wavelength fluctuations and aligns a spectrum correctly at 296.728 nm, and Step 2 corrects for monochromator non-linearities that remain fairly constant throughout a season.

From an examination of the approximately 300-500 Mercury scans recorded during a season, ***three sources*** of uncertainty in the wavelength alignment appear.

First, there may be wavelength fluctuations within one day, which cannot be detected by wavelength scans that are usually performed only once a day. (These fluctuations were more pronounced in the first years of network operation and therefore, more than one wavelength scan was carried out per day during this period). These variations can be attributed to power failures of the instrument, loss of index in the stepping motor, thermal expansion of the monochromator due to slight temperature variations, other mechanical causes, and random noise in the peak-finding algorithm. Typically, the variation in the position of the 296.728-nm line is less than ±0.02 nm between consecutive wavelength scans and this value is therefore also a good estimate of the wavelength variation during one day. Figure 3.14 shows the distribution of the wavelength deviation from the 296.728-nm line for Palmer Volume 7. The figure is based on all wavelength scans performed in the 1997/98 season.

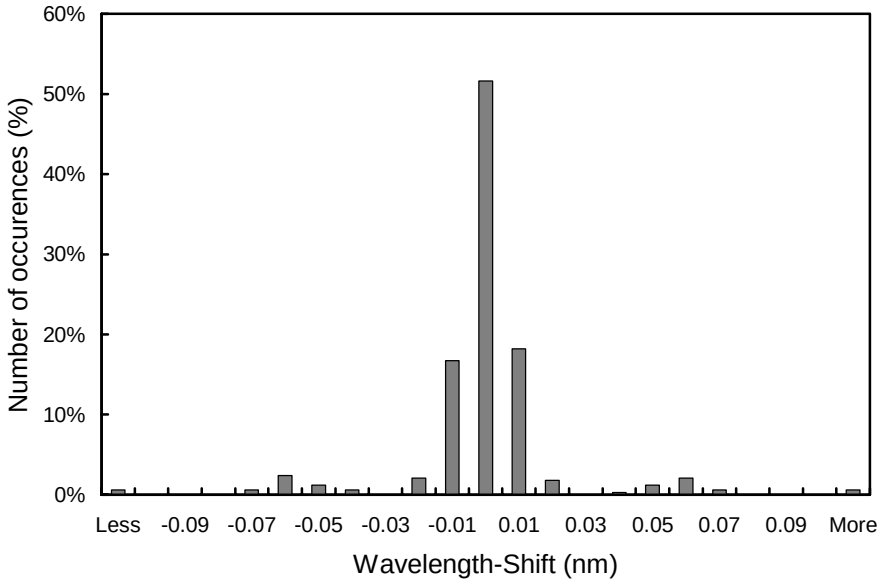

Figure 3.14. *Differences in the measured position of the 296.728 nm Mercury line between consecutive wavelength scans for Palmer Volume 7. The x-labels give the center wavelength shift for each column. Thus, the 0-nm histogram column covers the range -0.005 to +0.005 nm. "Less" means shifts smaller than –0.105 nm; "more" means shifts larger than 0.105 nm. For 90% of the days, the change in offset is smaller than ±0.025 nm.*

The **second** source of uncertainty is caused by changes in monochromator non-linearity during a season. As mentioned before, one function is usually applied for the whole season. (At some sites two or three functions have been applied historically. This is usually necessary if an instrument was removed and serviced during a season). The uncertainty caused by this approach is given by the standard deviation of the variation of individual wavelength scans. In the UV-B, the standard deviation (1σ) is generally less than 0.01 nm, and increases to 0.05 nm in the visible. The uncertainty in the UV-B is lower because most of the fluctuations are removed by Step 1 described above.

A **third** source of error in the wavelength domain occurs due to the different optical light paths for internal wavelength scans and measurements of solar irradiance. As described above, this effect can be tracked by comparing internal and external wavelength scans. The different geometry introduces a bias into the data that is usually constant throughout an operating season but varies from site to site. For example, during the 1995-1997 season, external wavelength scans were performed during opening and closing site visits at all sites. While opening and closing scans exhibited consistent results, variations from site to site were up to 0.05 nm, as measured by the offset of the 296.73 nm spectral line. The difference in the 296.73-nm line offset, calculated from external and internal wavelength scans, was 0.1 nm for Ushuaia and Palmer, and 0.14 nm for the South Pole. Figure 3.15 shows how the difference between both scan types may depend on wavelength. The difference at 296.73 nm is about 0.1 nm, increases to about 0.13 nm at 400 nm, and is about 0.05 nm in the visible.

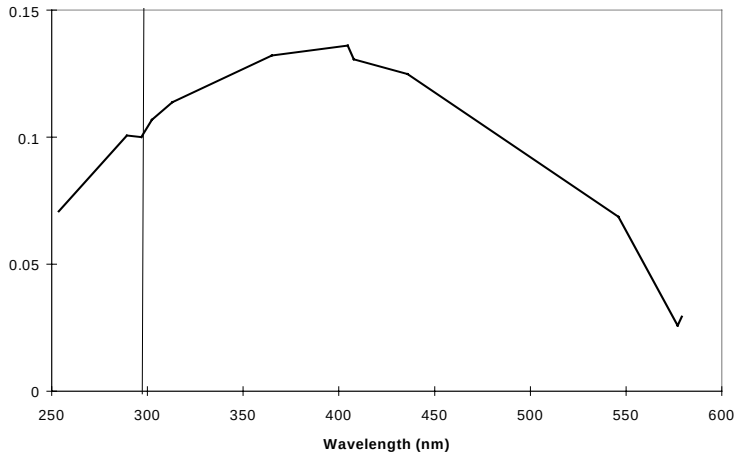

Figure 3.15. *Typical difference between the monochromator corrections based on external and internal mercury scans. The vertical line emphasizes the difference at 296.73 nm.*

This bias has not been corrected in any of our previously published datasets (i.e., Volume 1 to 6). For the current 1997/98 season, the problem has been addressed by implementing a method described in the next section. In order to give data users a feeling of how much the data have been affected in the past, a subset of San Diego Volume 7 data has been wavelength corrected with both the historic and new methods. A comparison of both datasets is compiled at the end of the Section 3.3.1.2.e.

3.3.1.2. Wavelength Calibration and Correction by the Fraunhofer-Correlation Method Implemented for Volume 7 Data

a) Principle of the correlation method

In order to improve the accuracy of the wavelength calibration and to avoid the problems associated with internal mercury scans, a new methodology was implemented for Volume 7. The method utilizes the Fraunhofer structure in solar spectra, which is caused by absorption processes in the Sun's outer atmosphere. This structure is also very marked in spectra of solar irradiance measured with the SUV-100 network radiometers, see Figure 3.2 for example. By correlating the structure in measured spectra with a similar structure in a reference solar spectrum (i.e., a spectrum with negligible wavelength errors) the wavelength shift can be determined and the measured spectra corrected. The method applied here is based on an implementation suggested by Slaper et al. (1995), Slaper (1997), and Slaper and Koskela (1997). The correlation-software (SHICrivm Version 2.7.) was provided by H. Slaper and was extended appropriately to match the data format and processing requirements of the NSF Network. The reference solar spectrum is based on a high-resolution (< 0.001 nm) extraterrestrial spectrum measured by the Fourier-Transform Spectroradiometer (FTS) at the National Solar Observatory (NSO) located at Kitt Peak, Arizona (Kurucz et al., 1984). The original spectrum was slightly modified by H. Slaper to account for an erroneous peak in the Kitt Peak spectrum in the 320-330 nm range (Slaper and Koskela, 1997). The wavelength accuracy of this spectrum has been proven to be better than 0.003 nm. The method has been successfully used to evaluate the results of several European intercomparison campaigns (Slaper et. al., 1995; Slaper, 1997; Slaper and Koskela, 1997; Reinen et. al., 1998; Seckmeyer et. al., 1998).

b) Advantages of the Fraunhofer-correlation method compared to wavelength alignment with external wavelength scans

As an alternative to the Fraunhofer-correlation method outlined above we could have also used external Mercury scans to improve the wavelength accuracy of Volume 7 data. For the following reasons we decided to use the correlation method:

1. In our implementation of the Fraunhofer-correlation method a wavelength shift value is provided every 10 nm between 300 and 440 nm giving 15 values in total. There are only four useable mercury lines in

the same spectral range. Thus the correlation method delivers corrections in much smaller wavelength increments. Since some monochromators deployed in the network show variations in linearity varying on a 20-nm scale the higher resolution of the correlation method improves overall correction accuracy.

2. At some sites only a few external wavelengths scans, exist since those scans are usually only performed during a site visit. With the correlation method, in contrast, the wavelength accuracy can be checked every day and even drifts during a particular day can be investigated.

3. Peaks from external wavelength scans are sometimes asymmetrical. Depending on the method applied, the center wavelength assigned to such a scan may vary by up to 0.15 nm, see Figure 3.12.

4. For the correlation method, we assume a symmetrical, triangular slit function with the same bandwidth as a typical external wavelength scans of the site under consideration. Using this approach, uncertainties due to asymmetrical slit functions are significantly reduced.

5. The correlation method can be fairly well automated; a separate evaluation of external scans is not necessary.

6. The correlation method uses the Sun as the calibration source. Therefore, the calibration source is the same for all sites. In future, the method could also be applied to data of previous seasons, which were recorded before wavelength scans with external Mercury lamps became available. Thus the time-series of network data could gain additional consistency.

c) Implementation of the correlation method

The objective of the implementation is to describe the monochromator non-linearity correction function with results from the Fraunhofer-correlation method rather than internal wavelength scans. The set of linear functions, which were calculated in Section 3.3.1.1 on the basis of internal Mercury scans (see Figure 3.13), will therefore be replaced by a set of similar functions derived from the Fraunhofer-correlation method. The advantage of this approach is that the software processing the data remains consistent with versions used in previous years; only the correction function changes.

Unfortunately, the Fraunhofer-correlation method can be used only in the wavelength range between 300 nm (310 nm for Barrow, McMurdo, and South Pole due to low solar elevations) and 440 nm. Below 300 nm, the signal is too noisy, i.e., the Fraunhofer structure in measured spectra is too distorted by noise to allow a reasonable correlation with the reference spectrum. Above 440 nm, the accuracy of the available reference spectrum is unknown and therefore we decided not to implement the method there.

In order to retrieve correction values outside the core-range of 300-440 nm we applied a combination of internal wavelength scans and the Fraunhofer-correlation method. In the first step, the mean deviation of wavelength shifts determined with internal wavelength scans and the Fraunhofer-correlation method is determined between 300 and 440 nm. For all sites the mean difference is between 0.08 and 0.15 nm, which is also consistent with the difference between internal and external wavelength scans. In a second step, the values of the internal wavelength scans outside the core-range (300-440 nm) are shifted by this average value. We estimate the accuracy of this method for wavelengths in the critical region around 300 nm to be better than 0.05 nm. For example, the shift values for the two neighboring wavelengths 300 nm (Fraunhofer-based) and 296.73 nm (based on shifted internal wavelength scan) usually agree to within 0.03 nm. For wavelengths above 440 nm, the wavelength accuracy is less critical (see the end of Section 3.2.1.1.) and therefore our approach is also appropriate for the visible.

The algorithm used to calculate the monochromator non-linearity correction functions consists of six steps:

1. Determine the wavelength shift of the 296.728 nm Mercury line from the daily internal wavelength scans and apply this shift to the data scans. Step 1 is similar as for the method described in Section 3.2.1.1, where the wavelength correction was solely based on internal scans. After this step, all data scans are aligned consistently at 296.728 nm. Due to the bias of internal wavelength scans, however, there is still an error in the wavelength alignment at 296.728. Step 1, however, is only intended to

homogenize the data set (i.e., remove day-to-day fluctuations) rather than eliminate the systematic bias.

2. Use the Fraunhofer-correlation algorithm to determine the wavelength-dependent wavelength shift in the homogenized data set (300-440 nm).

3. Compare the wavelength-shifts determined with the Fraunhofer-correlation method with the shifts apparent in internal Mercury scans, calculate the mean deviation, and shift the values from the internal wavelength scans *outside* the core-interval (i.e., $\lambda < 300$ nm or $\lambda > 440$ nm) by this shift value.

4. Establish a set of linear equations describing the monochromator non-linearity function. Usually, only one function is needed per site and season.

5. Apply the wavelength correction to all data.

6. Check the result of the wavelength correction by running the Fraunhofer-correlation method again.

Figure 3.16 illustrates two functions expressing the monochromator non-linearity that were determined for the Barrow instrument. The lower curve is based on the "old-fashioned" method, i.e., only internal Mercury scans have been evaluated. The upper curve was generated with the new Fraunhofer-correlation method. As described above, a pure Fraunhofer correlation was applied in the core range of 310-440 nm and the values outside this range are based on shifted internal scans. The difference between both curves is about 0.12 nm. The graph is based on data from the current 1997/98 season and the upper curve represents the correction function that was actually applied to the Barrow data of this season. Using one function for the whole season is justified because monochromator non-linearities were very stable throughout the year, as indicated by the error bars in Figure 3.16. These represent the 2σ standard deviation of the monochromator non-linearity and were calculated from all noontime scans recorded during the season.

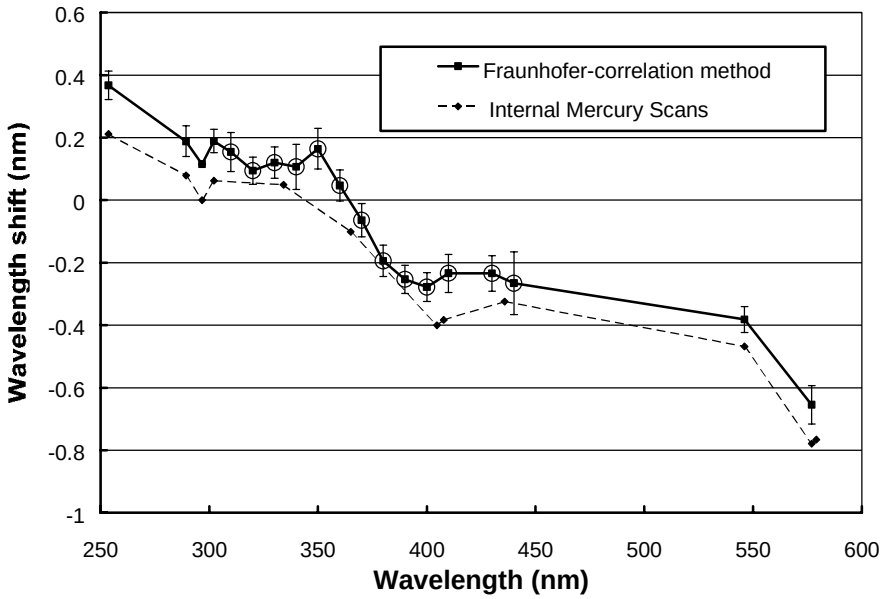

Figure 3.16. *Monochromator non-linearity correction function for Barrow Volume 7. Dashed line: Function calculated solely with internal Mercury scans. Solid line: Function calculated with a combination of results from the Fraunhofer-correlation method and internal Mercury scans. Between 310 and 440 nm the function is based on the Fraunhofer-correlation method only (marked with circles in the plot). Outside this interval, the function is based on internal Mercury scans, which were shifted by the mean difference between both methods. See text for a more detailed description. Both functions represent average wavelength shifts for the 1997/98 season. The error bars give the 2σ standard deviation variation of the wavelength shifts.*

d) Quality control of the Fraunhofer correlation method

After the data were corrected, the residual wavelength shifts were again determined with the Fraunhofer-correlation algorithm. The result is shown in Figure 3.17. For wavelengths between 320 and 440 nm, the shift is generally smaller than ±0.1 nm, with a few exceptions. The 310 nm shifts show a larger deviation in 1997 and early in 1998. However, these more pronounced shifts are not due to the instrument. At these parts of year, solar zenith angles are rather large and measurements at 310 nm are only slightly above the detection limit. Thus the correlation method is affected by noise in the data leading to erroneous results.

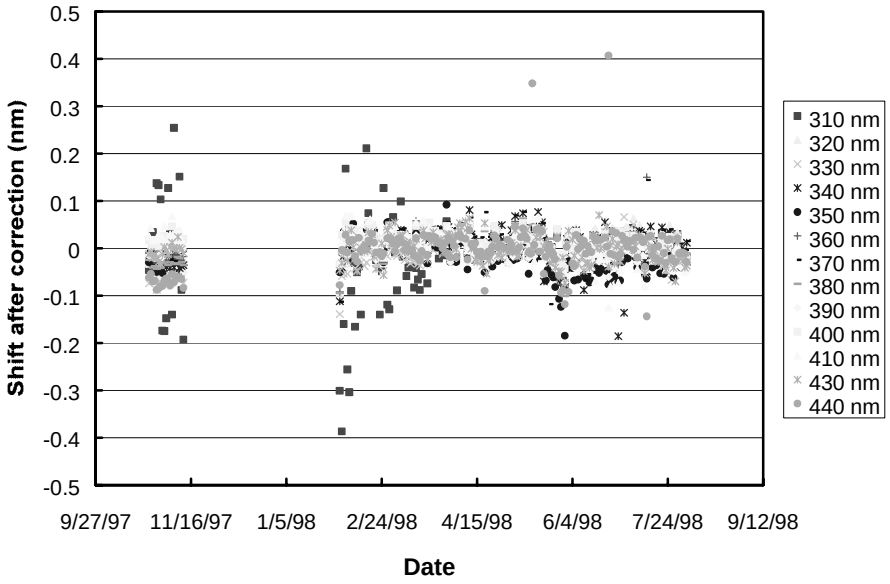

Figure 3.17. *Check of the wavelength alignment of the Barrow Volume 7 data after applying the Fraunhofer-correlation-based wavelength correction. The check was performed with the method developed by Slaper et al. (1995) using noontime spectra from the 1997/98 season. Similar results have been obtained for all sites.*

The check of the wavelength alignment presented in Figure 3.17 is not a complete evaluation of the absolute wavelength accuracy of the Barrow 1997/98 data. Both the calculation of the correction function and the check after applying the correction were performed with the same algorithm based on the work of Slaper et al. (1995). Therefore the wavelength alignment can be still affected by systematic errors introduced by this algorithm or its reference spectrum. According to Slaper and Koskela (1997), the estimated alignment uncertainty of the method is "probably less than 0.02 nm for instruments with a FWHM of 1 nm or less." However, features in the measured spectra, which are not caused by the Fraunhofer structure (e.g., changes in the wavelength increment and pauses when the PMT high-voltage changes), may confuse the algorithm. We therefore also checked the wavelength-corrected data set with an independent implementation of a Fraunhofer-correlation method that had been developed by Mayer (1997). The reference spectrum of this method is an extraterrestrial spectrum measured by the Solar Ultraviolet Spectral Irradiance Monitor (SUSIM) during the third space shuttle mission of the Atmospheric Laboratory for Applications and Science (ATLAS 3). The original spectrum can be obtained from the ftp server *ftp://susim.nrl.navy.mil*. The spectrum is given in vacuum-wavelengths and was shifted to air-wavelength before its use in the correlation algorithm.

Figure 3.18 shows the result of the check with the method developed by Mayer (1997). Between 310 and 400 nm, the deviations are smaller than ±0.1 nm with only few outliers. As expected, the wavelength shifts are slightly larger than those presented in Figure 3.17. Deviations of both methods of about 0.02 nm have also been reported by Seckmeyer et al. (1998). The deviations are still sufficiently small to give confidence in the wavelength correction. We therefore have implemented the Fraunhofer-correlation method at all sites for Volume 7 data.

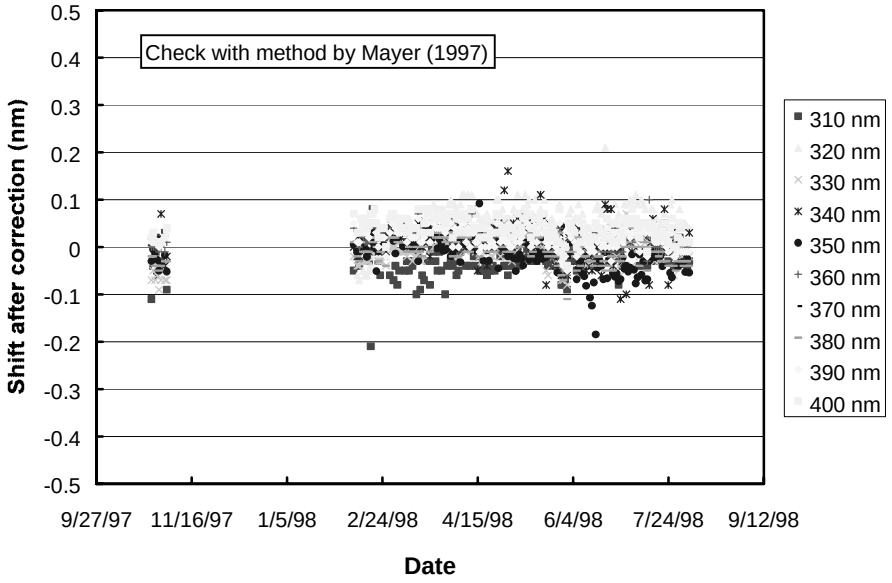

Figure 3.18. *Check of the wavelength alignment of the Barrow Volume 7 data after applying the Fraunhofer-correlation-based wavelength correction. The check was performed with the method developed by Mayer (1997).*

e) Comparison of the historic wavelength correction method with the Fraunhofer-correction method

In order to quantify the effect of the change in the wavelength correction method on solar irradiance data, a subset of San Diego Volume 7 data (days 9/9/97-12/31/97) was corrected with both the historic and the new procedures. Figure 3.19 shows the ratio historic correction/new correction for several irradiance integrals versus solar zenith angle. The difference in both datasets depends significantly on wavelength. For example, the integral 400-600 nm is almost independent of the wavelength correction applied (i.e., the ratio is about 1.0), while differences for the 303.03-307.692 nm integral can be as high as 6.5%. This behavior can be expected because the latter integral includes wavelengths in the UV-B, where ozone absorption leads to a large change of spectral irradiance with wavelength. The ratio for this short-wave UV-B integral is always smaller than 1.0. This means that a wavelength correction with the historic method, which was applied for Volume 1-6 data, leads to lower irradiances than a correction with the Fraunhofer method. This can also be concluded from the direction of the shift between internal and external Mercury scans.

Figure 3.19 also includes a comparison of both correction methods for two biological dose rates, erythemally weighted irradiance and DNA-weighted irradiance. At 50° SZA, values corrected with the old method are lower by 2% and 4% for erythemal and DNA irradiance, respectively. For DNA-weighted irradiance, the difference is almost independent of SZA, whereas the difference for erythemal values appears to be smaller at larger SZA. This SZA-dependency is quite different from the behavior of the 303.03-307.692 nm integral mentioned earlier. For this integral, the difference at 30° SZA is about 4%. At 75° SZA, the difference increases to 6.5% and then diminishes again towards larger SZAs. The reason for this change with SZA is the different "shape" of the solar spectrum at different solar elevations.

The magnitude of the difference between both correction methods agrees very well with theoretical evaluations published by Bernhard and Seckmeyer (1999). In this paper, formulas are given to calculate the effect of wavelength shifts on biologically weighted irradiance as well as on spectral irradiance at a specific wavelength. The formulas require as input parameters the magnitude of the wavelength shift, SZA, total column ozone, and the action spectrum under consideration. We applied these formulas to San Diego data by setting the wavelength shift to 0.109 nm (the average difference between internal and external

wavelength scans for the San Diego instrument in late 1997), and total column ozone to 300 DU (approximately the average total column ozone for San Diego). The results are indicated in Figure 3.19 with large symbols. As can be seen, the theoretical results fit quite well to the experimental data, both in magnitude and SZA-dependency. For example, the increase of the ratio historic correction/new correction for erythemal irradiance towards larger SZA is also reflected in theoretical results (compare small and large diamond symbols in Figure 3.19). Similarly, the bowl-shaped ratio of the 303.03-307.692 nm integral is confirmed by the theoretical values (square symbols).

The data presented in Figure 3.19 are from San Diego only and may not be representative for high latitude sites, where total column ozone is quite different from the prevailing values for San Diego. This is particularly the case in September and October when the ozone hole affects measurements at the Austral sites. According to Bernhard and Seckmeyer (1999), however, the influence of column ozone on systematic errors in biologically weighted irradiances caused by wavelength shifts is usually below 0.5%. The results from San Diego can therefore also be applied to the other network sites.

In conclusion, biological doses published in earlier Volumes appear to be too low by approximately 2-4%, almost independent on solar zenith angles, if the same shift between "internal" and "true" wavelength existed as for the San Diego instrument. The systematic errors in short-wave UV-B irradiances, like the 303.03-307.692 nm integral, may be larger and, in addition, SZA-dependent. On the other hand, integrals in the UV-A and visible are insignificantly affected by the systematic error introduced by the historic wavelength correction method, which was based on internal Mercury scans only.

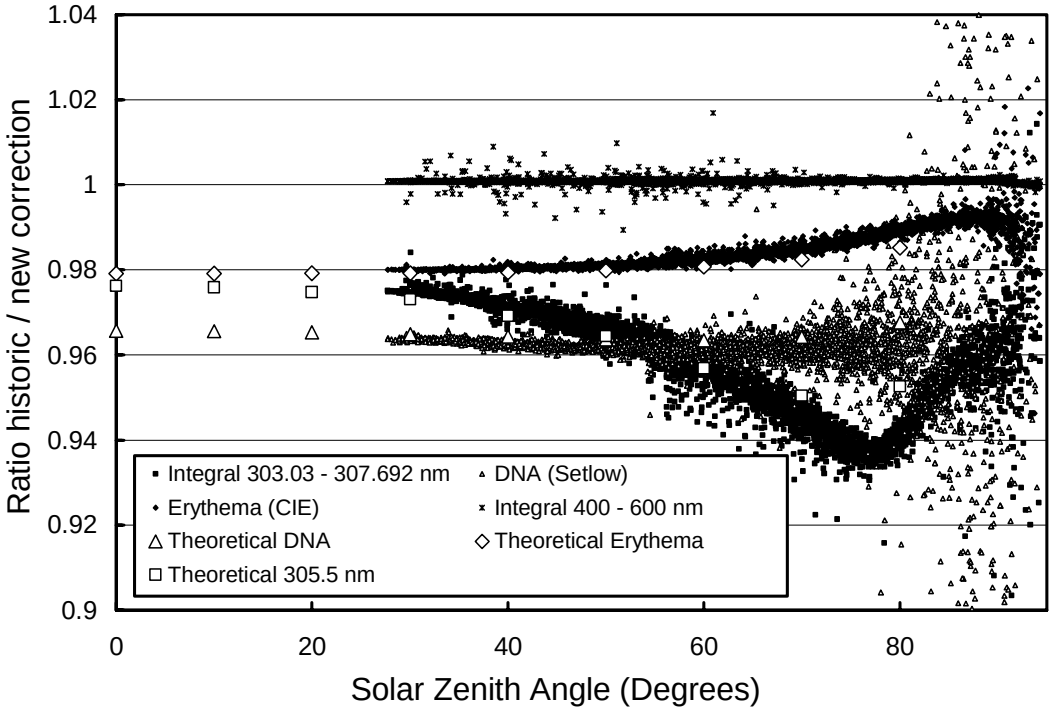

Figure 3.19. *Effect of the wavelength correction method on spectral integrals. Small symbols show the ratios of data, which were corrected with the historic mercury scan-based method, to data corrected with the new Fraunhofer method. Four different data products are depicted, including the 303.03-307.692 nm and 400-600 nm integrals, as well as erythemally and DNA-weighted irradiance. Large symbols show theoretical results according to Bernhard and Seckmeyer (1999). See text for details.*

3.3.2. Irradiance Calibration

At each instrument site, an irradiance (or absolute) calibration is performed approximately biweekly to transfer a calibration to the internal response lamp. This section describes how

- The values in calibration certificates of 200-Watt Standards of Spectral Irradiance are interpolated (Section 3.3.2.1.)
- The internal response lamp is calibrated (Section 3.3.2.2.)
- The system responsivity is determined and solar data is calibrated (Section 3.3.2.3.)
- Different 200-Watt standards are intercompared (Section 3.3.2.4.)
- A calibration is transferred to a 200-Watt spare standard (Section 3.3.2.5.)

Most quantities used for these calculations are defined in **Table 3.2**.

Table 3.2 Data processing parameters.

V	PMT high voltage setting for the photomultiplier tube (PMT)
λ	Wavelength
$I_{dark}(\lambda,V)$	Mean PMT dark current for a given PMT high voltage
$I_{ext}(\lambda,V)$	PMT current during a absolute scan as a function of wavelength and PMT high voltage
$I_{int}(\lambda,V)$	PMT current during a scan of the internal response lamp
$I_{solar}(\lambda,V)$	PMT current during a standard data scan of sunlight
$E_{interp}(\lambda)$	Interpolated irradiance values of a 200-Watt standard of spectral irradiance calculated from the (NIST traceable) calibration certificate of that lamp
$E_{int}(\lambda)$	Apparent irradiance of the internal response lamp as a function of wavelength
$E_{solar}(\lambda)$	Unknown (or solar) irradiance as a function of wavelength
$R(\lambda,V)$	System responsivity; normally a function of wavelength and PMT high voltage

The following effects may influence a correct irradiance calibration:

1. A 200-Watt standard of spectral irradiance has changed its intensity between its factory calibration and its use on-site.
2. The entrance optics have changed between external calibrations with 200-Watt lamps.
3. The internal response lamp has changed.

Using two or more different lamps on-site minimizes uncertainties because of (1). Additionally, a traveling Standard of Spectral Irradiance is brought to the site during annual site visits and the calibrations of all lamps are intercompared. By evaluating the results of the biweekly 200-Watt calibrations, possible changes in the entrance optics and/or other system components can be checked and the system responsivity can be adjusted accordingly. The stability of the internal response lamp is tracked by the external 200-Watt calibrations, the internal "TSI" sensor, and by monitoring the drive current during use of the lamp.

3.3.2.1. Interpolation of Values in Certificates of 200-Watt Standards

The irradiance calibration of the spectroradiometers is based on Standards of Spectral Irradiance purchased from Optronics Laboratories. These are 200-Watt tungsten-halogen lamps of type Q6.6AT4/5CL from General Electric. Their calibration is traceable to standards maintained by the National Institute of Standards and Technology (NIST). The lamps are calibrated by Optronics Laboratories in an alignment

fixture matching that used at the sites, both in orientation (downward light path) and distance. In order to calibrate an SUV-100 spectroradiometer, the 200-Watt lamps are periodically mounted on top of the instrument and scanned (see Section 3.2.4).

The Standards of Spectral Irradiance are provided by the manufacturer with a table of irradiance values in 10-nm increments. To provide irradiance values in smaller wavelength increments, for use with wavelengths obtained during the calibrations, a Black-Body function (or Planck equation) is used:

$$E_{\text{interp}}(\lambda) = a\frac{2hc^2}{\lambda^5}\frac{1}{\exp\{\frac{hc}{k\lambda T}\}-1}$$

where h is Planck's constant, c is the velocity of light, k is the Boltzmann constant, and T is the temperature in Kelvin. The term a is a scale factor. An equation fitting routine is used to adjust terms a and T throughout the region [290, 600] nm to yield the best fit to the manufacturer's (NIST-traceable) data, as shown in Figure 3.20.

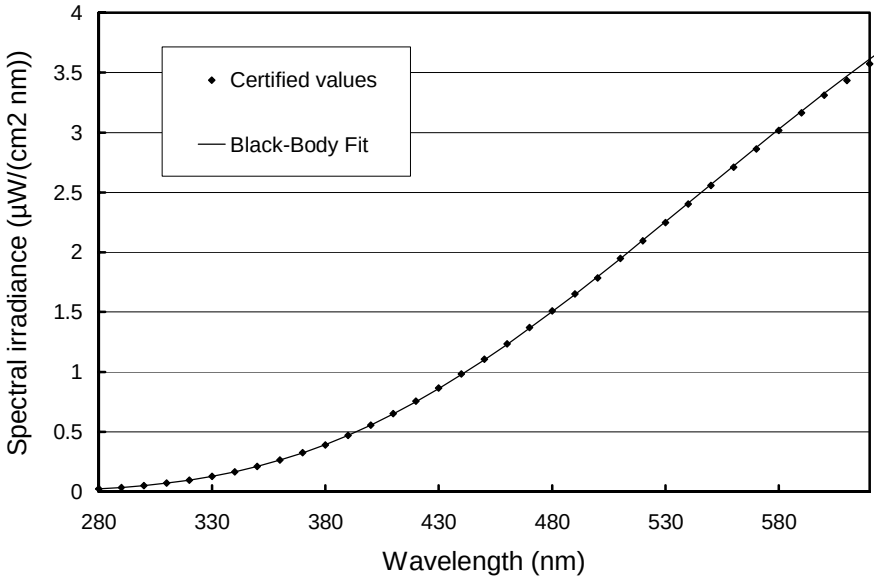

Figure 3.20. *Spectral Irradiance of the San Diego site standard 200W010. The dots are the values from the lamp's certificate provided by Optronics Laboratories. The line through these points is the Black-Body fit.*

Since a lamp spectrum does not perfectly agree with a Black-Body function, the fit will introduce an error, which is in general less than ±1%. Figure 3.21 shows the ratio of the Black-Body fit values and the certified values of the San Diego site standard 200W010. Both data sets agree to within ±1%, demonstrating that the fit method chosen is reasonably accurate.

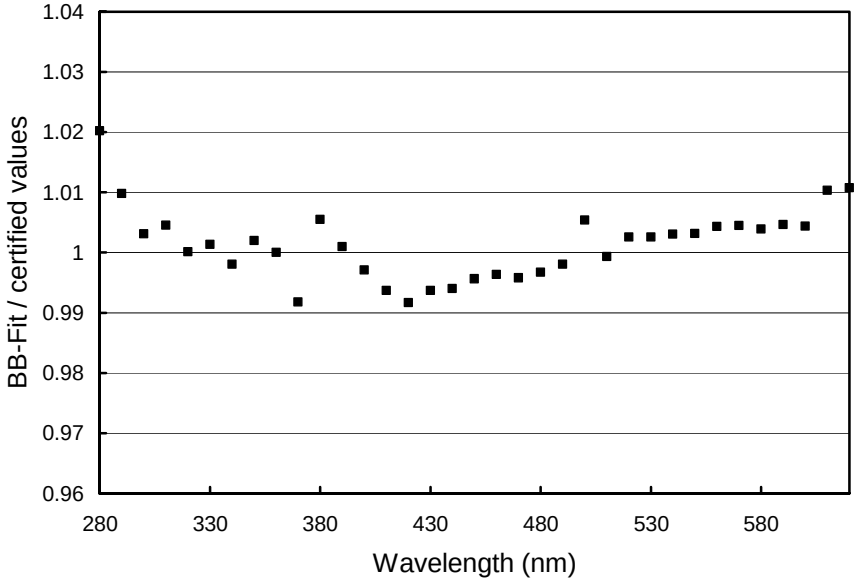

Figure 3.21. *Ratio of the Black-Body fit values and the certified values of the San Diego site standard 200W010. Both data sets agree to within ±1%. The graph is based on the same values as shown in the previous figure.*

3.3.2.2. Calibration of the Response Lamp

A system irradiance calibration consists of the transfers of the calibration from a 200-Watt lamp to the internal response lamp. For this procedure, the 200-Watt lamp is positioned in a specially designed lamp stand outside the roof box such that the distance from the lamp filament to the diffuser of the SUV-100 spectroradiometer is 50 cm, as specified in the calibration certificate of the 200-Watt lamp. The output of the system, I_{ext}, is recorded (in nA) as a function of wavelength, λ, and PMT high voltage, V. Immediately after the scan of the external lamp, the shutter is closed, a warm-up period for the response lamp occurs, and a scan is made with the response lamp at the same PMT voltage as previously applied for the 200-Watt lamp scan. Parallel short dark scan segments are also recorded with both lamps off. Following this procedure, a wavelength scan is performed and both 200-Watt and response lamp scans are shifted in wavelength accordingly. Subtracting dark values from the appropriate PMT current, the apparent irradiance of the response lamp, E_{int}, is calculated:

$$E_{\text{int}}(\lambda) = E_{\text{ext}}(\lambda)\frac{I_{\text{int}}(\lambda,V) - I_{\text{dark}}(V)}{I_{\text{ext}}(\lambda,V) - I_{\text{dark}}(V)}$$

Note that E_{int} is not a "true" irradiance produced by the internal lamp at the place of the entrance optics but acts as a reference value when comparing the irradiance produced by the external lamp and solar irradiance.

Each biweekly calibration with a 200-Watt Standard of Spectral Irradiance provides a function $E_{\text{int}}(\lambda)$. Ideally, these functions should not change from one calibration event to the next. In reality, there are changes due to following reasons:

- The response lamp has drifted, i.e., the lamp became darker or brighter.
- Calibrations are performed with different 200-Watt lamps.
- Random changes in the alignment of the lamp, the lamp current, or the lamp itself.

For these reasons, calibration of the spectroradiometer in a given time period is not based on one calibration event only. Instead, an average response lamp irradiance $\langle E_{\text{int}}(\lambda)\rangle$ is calculated from n

calibrations performed in time-intervals ranging from days to months, depending on the stability of the response lamp:

$$< E_{\text{int}}(\lambda) >= \frac{1}{n} \sum_{n} E_{\text{int},n}(\lambda)$$

In the following, $<E_{int}(\lambda)>$ is denoted "mean-irradiance of the response lamp". By this averaging, the influence of differences in the 200-W standards and random errors are reduced. If a response lamp drifts, however, the number of scans contributing to the average has to be limited in order to avoid systematic errors. The allowed drift of the lamp is typically 2%. If the drift in a given period is larger, the period is broken in two or more parts with one mean-irradiance $<E_{\text{int}}(\lambda)>$ calculated for each part. A whole season may be broken into as many as eight parts. For example, the same mean-irradiance was applied to the Volume 7 McMurdo data because of the very good stability of the response lamp, while Ushuaia's Volume 7 season consists of five time-periods, with a different mean-irradiance applied in each period.

3.3.2.3. Determination of the System Responsivity and Calibration of Solar Data

The calculation of solar spectral irradiance at a particular time requires the appropriate data scan, a response scan, and a wavelength scan. Response and wavelength scans are typically taken from the same date as the data scan or those scans closest in time to the data scan. In the first step, data and response scan are shifted in wavelength based on the wavelength scan and the table, which holds the mapping of the monochromator non-linearity. For Volume 1- 6, this table was based on internal wavelength scans, see Section 3.3.1.1.; for Volume 7, it is based on the Fraunhofer-correlation method described in Section 3.3.1.2. After all scans have been wavelength calibrated, the responsivity R of the spectroradiometer is calculated:

$$R(\lambda, V) = \frac{I_{\text{int}}(\lambda, V) - I_{\text{dark}}(V)}{< E_{\text{int}}(\lambda) >}$$

Note that R is determined separately for each PMT high voltage setting. $I_{\text{dark}}(V)$ is calculated from the 280-290 nm portion of the data scan that the response scan is paired with. The denominator $<E_{\text{int}}(\lambda)>$ is the response lamp's mean-irradiance, defined in the last section.

The solar spectral irradiance, E_{solar}, is finally calculated from the PMT currents in the data scan:

$$E_{\text{solar}}(\lambda) = \frac{I_{\text{solar}}(\lambda, V) - I_{\text{dark}}(V)}{R(\lambda, V)}$$

A typical solar irradiance spectrum retrieved with this procedure was already shown in Figure 3.2.

3.3.2.4. Comparison of Standards of Spectral Irradiance

A solar irradiance spectrum calculated with the procedure outlined above is only correct if the irradiance produced by the 200-Watt standard of spectral irradiance matches the values in the calibration certificate of the lamp. A mismatch can result from a variety of reasons including:

- The 200-Watt lamp became darker or brighter since its calibration at a standards laboratory.
- The irradiance scale preserved by Optronics Laboratories may change over time. Standards purchased in different years may therefore have a different calibration.
- Alignment errors; for example, the distance between lamp and entrance optics does not accurately match the target distance specified in the lamp's certificate.

- Thermal effects
- Operator error

To verify the calibration of the irradiance standards deployed at the different network sites, a visiting Biospherical Instruments Inc. engineer conducts a comparison of all on-site lamps with a "traveling" standard during the yearly site visits. Based on these data, we determine if significant changes have occurred in site lamps. For the 1997/98 season, each site was equipped with three standards. Historically, there were only two standards, a primary site standard and a "spare" lamp that did not have a calibration from a standards laboratory. Instead, a calibration was transferred to the spares by personnel from Biospherical Instrument applying a procedure outlined in Section 3.3.2.5.

The comparison of 200-Watt lamps is based on the fact that the spectral irradiance $E_{int}(\lambda)$, which is assigned to the response lamp, should not depend on the 200-Watt lamp used for its calibration. Let us assume that the response lamp is calibrated independently with two different 200-Watt standards, lamp #1 and #2. One standard is brighter than the other and this difference is accurately reflected in the lamps' certificates. In this case, the brighter lamp will lead to a larger PMT current, $I_{ext}(\lambda)$. The irradiance assigned to the internal lamp, $E_{int}(\lambda)$, however, will not depend on the 200-W lamp used because the values in the calibration certificate are higher by exactly the same amount. On the other hand, if there is a mismatch between the actual irradiance and the irradiance tabulated in the certificate of a 200-Watt lamp, $E_{int}(\lambda)$ will depend on the lamp used for the calibration. In more detail, the ratio $C(\lambda)$ between $E^{(1)}{}_{int}(\lambda)$, determined with lamp #1, and $E^{(2)}{}_{int}(\lambda)$, determined with lamp #2, allows us to quantify the difference between both calibration standards:

$$C(\lambda) = \frac{E_{\text{int}}^{(1)}(\lambda)}{E_{\text{int}}^{(2)}(\lambda)} = \frac{E_{\text{ext}}^{(1)}(\lambda)\dfrac{I_{\text{int}}^{(1)}(\lambda,V) - I_{\text{dark}}(V)}{I_{\text{ext}}^{(1)}(\lambda,V) - I_{\text{dark}}(V)}}{E_{\text{ext}}^{(2)}(\lambda)\dfrac{I_{\text{int}}^{(2)}(\lambda,V) - I_{\text{dark}}(V)}{I_{\text{ext}}^{(2)}(\lambda,V) - I_{\text{dark}}(V)}}$$

Only the definition of $E_{int}(\lambda)$, applied separately for lamp #1 and #2, was used in the above formula. If lamps #1 and #2 completely agreed with their certificates, $C(\lambda)$ would be 1. In order for the intercomparison to be valid, it is important that all scans involved are performed under the same conditions, i.e., the internal PMT currents $I_{\text{int}}^{(1)}(\lambda,V)$ and $I_{\text{int}}^{(2)}(\lambda,V)$ have to be identical, indicating stability of the internal response lamp.

Figure 3.22 shows a comparison of the 200-Watt standards 200W010 (Lamp #1) and M-874 (Lamp #2). Lamp 200W010 is one of the San Diego standards for Volume 7 and lamp M-874 is the traveling standard of the Volume 7 season. Both lamps were calibrated by Optronic Laboratories in September 1998. The comparison was performed on 9/3/97. In Figure 3.22, the function $C(\lambda) - 1$ is depicted. Ideally, the curve should equal the 0% line. In reality, the function deviates by approximately 5% in the UV and by 2% in the visible. A thorough investigation revealed that lamp 200W010 had drifted over time and that it was darker on the comparison day 9/3/97 compared to September 1998, when it was (re)calibrated. A darkening of the lamp leads to a smaller PMT-current $I_{\text{ext}}^{(1)}(\lambda,V)$. If $I_{\text{ext}}^{(1)}(\lambda,V)$ is low, $C(\lambda) - 1$ becomes larger than one, according to the equation above. This is in agreement with Figure 3.22. If the system had been calibrated with lamp 200W010 rather than M-874 solar measurements would become higher. More details on lamp 200W010 and its history are given in Section 5.7.

A lamp drift of 5% within two years is unusually high. Normally drifts of calibration standards are less than 2% per season. Some of the standards, which have been deployed for Volume 7, have two sets of calibration certificates from Optronics Laboratories. It is therefore possible to track the drift of these lamps

over time. Table 3.3 shows calibration information and amount of drift for all lamps that were used in the 1997/98 season.

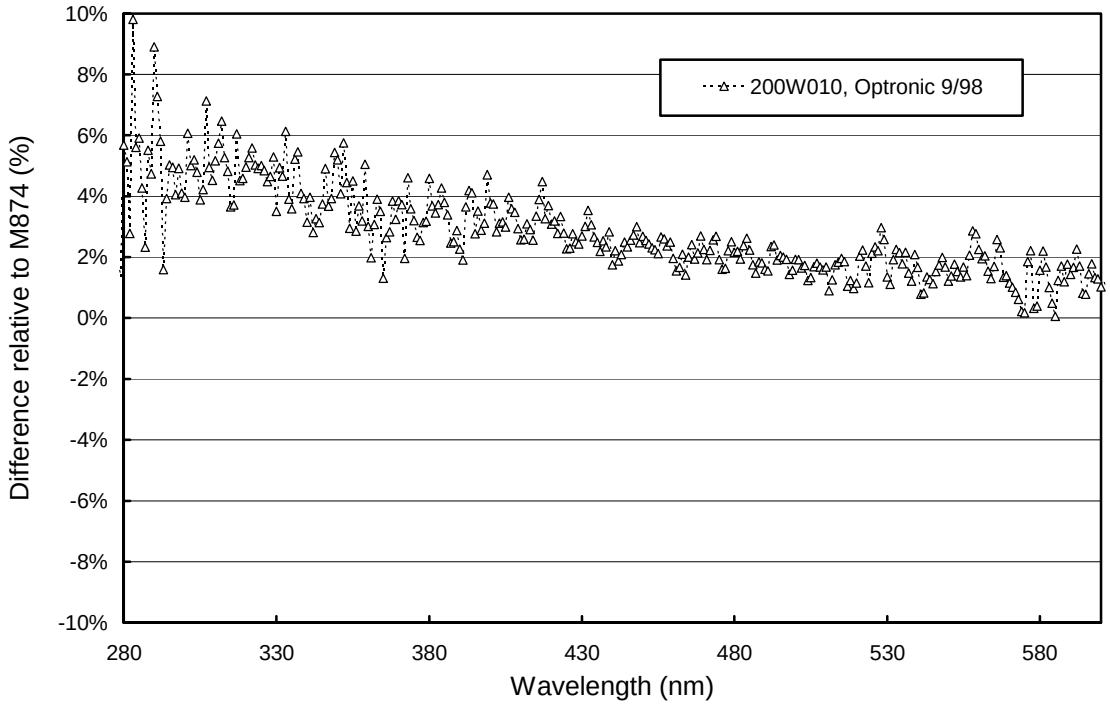

Figure 3.22. *Comparison of lamps 200W010 and M-874 expressed by the function C(λ) –1 . See text for details. The difference relative to M-874 is positive. This means that solar measurements would increase if 200W010, rather than M-874, were used for calibration.*

Table 3.3 Calibration standards used in the 1997/98 season*.

Site	Standard	Calibration 1	Calibration 2	Change between Calibration 1 and 2		
				@ 300 nm	@ 400 nm	@ 600 nm
Traveling Standard	M-874	Optr. 8/95 **	Optr. 9/98 **	+2.7%	+2.0%	+2.0%
McMurdo	M543	not used				
	M-764	Optr. 10/92				
	200W005	Optr. 11/96				
Palmer	M-700	BSI transfer				
	M-765	Optr. 10/92				
	200W007	Optr. 11/96				
South Pole	M-763	Optr. 10/92	BSI transfer from M-874 (Optr. 8/95)	+4%	+4%	+4%
	200W006	11/96				
Ushuaia	M-698	BSI transfer from M-874 (Optr. 9/98)				
	M-766	Optr. 10/92	BSI transfer from M-874 (Optr. 9/98)	+4.1%	+3.9%	+3.6%
	200W008	Optr. 11/96				
Barrow	M-699	Optr. 9/98				
	M-762	Optr. 10/92	Optr. 9/98	+2.2%	+1.9%	+1.4%
	200W009	Optr. 9/98				
San Diego	M-881	Optr. 8/95	Optr. 9/98	+3.2%	+2.8%	+1.0%
	200W010	Optr. 11/96	Optr. 9/98	+9.6%	+5.7%	+3.9%
	200W009	Optr. 9/98				

**Some lamps have more than one calibration. The difference between these calibrations is marked in the three rightmost columns (positive change means that Calibration 2 revealed higher irradiance values). The calibrations that were actually used in the season are shaded.*

*** The 8/95 Optronic Laboratories certificate of the traveling standard M-874 was used for McMurdo and South Pole, since the Volume 7 time periods for these sites are closer to the 8/95 calibration than for the other sites. For Palmer, Ushuaia and Barrow, the 9/98 Optronic Laboratories certificate of the traveling standard M-874 was used. For San Diego, a third calibration of M-874 was implemented in the first part, and the 9/98 Optronic Laboratories certificate was used in the remainder of the season. See Section 5.7. for more details on the San Diego calibration.*

Although the above figure and table are not exact estimates of lamp drifts, they do give an indication of lamp calibration uncertainties, which appear to exceed the 1.5% uncertainty published by the lamp calibration service provider Optronic Laboratories. All lamps appeared to be brighter during the Optronic Laboratories calibration in 1998 compared to previous calibrations. Comparisons of the traveling standard M-874 with other standards on site indicate that the lamp actually became brighter by about 2% between January 1998 and September 1998, when the lamp was recalibrated. This change of the lamp's brightness is in agreement with the difference between the 1995 and 1998 calibrations by Optronic Laboratories.

3.3.2.5. Calibration of Spare Lamps

Not all lamps on site have a calibration certificate from Optronic Laboratories or another calibration facility. It is therefore necessary to transfer a calibration from a calibrated lamp to these "spare lamps." To

calibrated a spare lamp (i.e. define its scale factor *a* and color temperature *T*), spare lamp and primary lamp are operated one after the other and spectral irradiance $E^{\text{spare}}(\lambda)$ of the spare lamp is then calculated by:

$$E^{\text{spare}}(\lambda) = E_{\text{int}}(\lambda)\frac{I^{\text{spare}}(\lambda,V) - I_{\text{dark}}(V)}{I_{\text{int}}(\lambda,V) - I_{\text{dark}}(V)},$$

where $I_{\text{int}}(\lambda,V)$ is determined with the primary lamp as outlined in Section 3.3.2.3. This formula, together with the values obtained from the measurements, gives an appropriate table for $E^{\text{spare}}(\lambda \in [280,600]\text{nm})$, which is used to define the coefficients *a* and *T* for the site spare as outlined above. This transfer of the irradiance from standard lamps to site spares increases the number of calibrated lamps at the sites and also provides some backup if the primary standard breaks or drifts.

3.3.3. Biological Dose Calculations

The impact of radiation on biological systems is usually described as the integral of the product of spectral irradiance, $E(\lambda)$, and a "biological weighting function" $W(\lambda)$:

$$E_{\text{bio}} = \int_{\lambda_1}^{\lambda_2} E(\lambda)W(\lambda)\,d\lambda$$

$W(\lambda)$ is also often denoted "action spectrum" and is a dimensionless function. In this report, we refer to E_{bio} as a "biological dose." Spectral data from the UV network are routinely processed to calculate biological doses according to several published weighting functions (see Figure 3. 23 a-b and Figure 3.24). The above integral is usually evaluated with the integration limits, λ_1 and λ_2, 286 and 400 nm, respectively. The integration is approximated via a sum with $d\lambda$ = 0.2 nm steps typically between 286 and 345 nm, and $d\lambda$ = 0.5 nm steps between 3450 and 400 nm, where applicable.

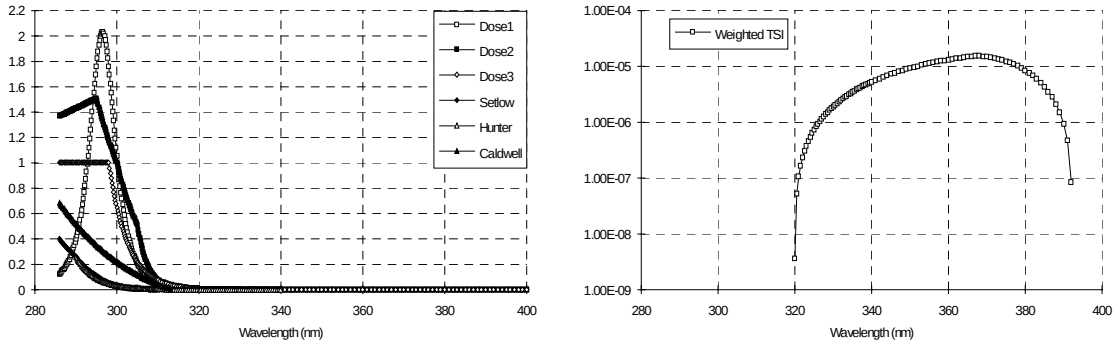

Figure 3. 23. a-b. *Biological weighting functions (linear axis) and spectral responsivity of the TSI (logarithmic axis).*

The data on CD-ROM includes six biological doses abbreviated by Setlow, Hunter, Caldwell, Dose1, Dose2, and Dose3_CIE_Erythema. The action spectra for these doses are described below and are plotted in Figure 3.24. The data of spectral irradiance were also weighted with the spectral responsivity of the TSI sensor and these data can be also found on CD-ROM. Please see the Appendix A5 for a detailed listing of the code used to compute biological doses from these weighting functions.

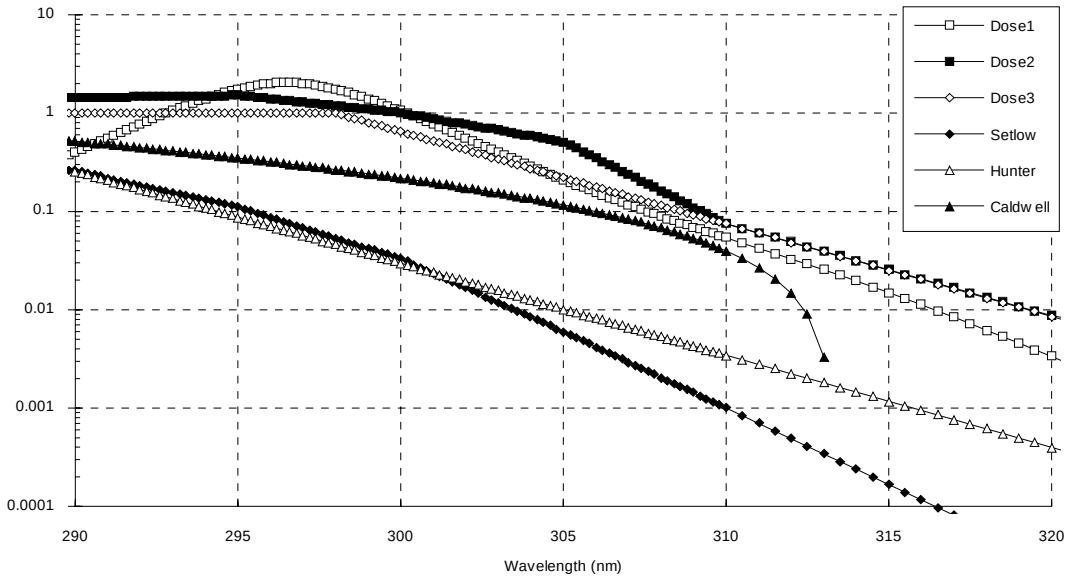

Figure 3.24. *Details of various biological- weighting functions. Note logarithmic scale axis.*

"Setlow" is based on a parameterization of the spectral dependence of damage to unprotected DNA that was suggested by R. B. Setlow (1974). The integration range is from 286 to 340 nm.

$$W(\lambda) = 10^{D(\lambda)}, \text{ where } D(\lambda) = \begin{cases} 13.04679 - 0.047012\lambda, 286 \le \lambda < 290 \\ 20.75595 - 0.073595\lambda, 290 \le \lambda < 295 \\ 30.12706 - 0.105362\lambda, 295 \le \lambda < 300 \\ 42.94028 - 0.148073\lambda, 300 \le \lambda < 305 \\ 45.24538 - 0.15563\lambda, 305 \le \lambda \le 340 \end{cases}$$

Please note that other parameterizations of Setlow (1974) exist. Care must be used in comparisons with other methods.

"Hunter" is based on an exponential function fit to the data of J.H. Hunter, J.H. Taylor, and H.G. Moser (1979) and reported in numerical form by R.C. Smith and K. S. Baker (1982). The integration range is from 290 to 340 nm.

$$W(\lambda) = \exp\{61.1381 - 0.21551\lambda\}$$

"Caldwell" refers to a parameterization of A.E.S. Green, T. Sawada, and E.P. Shettle (1974) for Caldwell's data on the relative photon effectiveness of UV-B irradiation to induce biological response, when protein or nucleic acid chromophores are involved (M. M. Caldwell, 1971). Integration range is from 286 to 313 nm.

$$W(\lambda) = 2.618 \cdot (1 - (\frac{\lambda}{313.3})^2) \cdot \exp\{\frac{300 - \lambda}{31.08}\}$$

"Dose1" refers to an action spectrum of erythema defined by W.D. Komhyr and L. Machta (1973). The parameterization used is found in A.E.S. Green, T. Sawada, and E.P. Shettle (1974). The weighting function peaks at 296.5 nm. The integration range is 286 to 400 nm. Note that a coding error exists in previous data sets (Volume 1-5) for this dose function; for more information see Section A6.

$$W(\lambda) = \frac{0.4485}{1 + \frac{\exp\{\lambda - 311.4\}}{3.13}} + \frac{4 \cdot 0.9949 \cdot \exp\{\frac{\lambda - 296.5}{2.692}\}}{1 + \exp\{\frac{\lambda - 296.5}{2.692}\}^2}$$

"Dose2" refers to an alternative action spectrum for erythema in human skin proposed by B.L. Diffey (1987). It is a multisegment power fit to tabular data.

$$W(\lambda) = 10^{D(\lambda)}, \text{ where } D(\lambda) = \begin{cases} -1.215837 + 0.004728\lambda, 286 \le \lambda < 295 \\ 10.73862 - 0.035795\lambda, 295 \le \lambda < 300 \\ 17.54579 - 0.058486\lambda, 300 \le \lambda < 305 \\ 50.49061 - 0.166502\lambda, 305 \le \lambda < 310 \\ 27.87686 - 0.093554\lambda, 310 \le \lambda < 320 \\ 15.3893 - 0.054531\lambda, 320 \le \lambda < 335 \\ 1.703584 - 0.013555\lambda, 335 \le \lambda < 365 \\ 8.365825 - 0.031808\lambda, 365 \le \lambda < 380 \\ -1.705338 - 0.005305\lambda, 380 \le \lambda \le 400 \end{cases}$$

Please note that this function peaks at 295 nm $\max_{\lambda} W(\lambda) = 1.51$.

"Dose3_CIE_Erythema" refers to the action spectrum for erythema in human skin proposed by McKinlay and Diffey (1987). This is the erythema action spectrum that is most widely used and it is often referred to as the "CIE action spectrum for erythema."

$$W(\lambda) = 10^{D(\lambda)}, \text{ where } D(\lambda) = \begin{cases} 0, 286 \le \lambda < 298 \\ -0.094(\lambda - 298), 298 \le \lambda < 328 \\ -0.015(\lambda - 139), 328 \le \lambda \le 400 \end{cases}$$

Note that this function equals "1" below 298 nm.

"Weighted TSI" is obtained by weighting spectral irradiance with the spectral responsivity of the build-in Total Scene Irradiance (TSI) sensor. The sensor consists of a filtered photodiode. The responsivity function was calculated from spectral transmission of the filter and spectral response of the diode. The integration range is 320 to 392 nm and the function is parameterized as follows:

$$W(\lambda) = \begin{cases} 0.005598382 - 0.04901834\frac{\lambda}{1000} + 0.1420638(\frac{\lambda}{1000})^2 - 0.1361036(\frac{\lambda}{1000})^3, \lambda < 367 \\ -0.08228739 + 0.6492523\frac{\lambda}{1000} - 1.70513(\frac{\lambda}{1000})^2 + 1.490757(\frac{\lambda}{1000})^3, \lambda \ge 367 \end{cases}$$

3.3.5. Sun Angles

All data in the databases on CD-ROM are accompanied by the specifications of solar zenith and azimuth angles at the middle of a data scan. Both angles were calculated according to an algorithm presented by Wilson (1980).